NASA CR-166679

EVALUATION OF THE EFFECTS OF VARYING MOISTURE CONTENTS ON MICROWAVE THERMAL EMISSIONS FROM AGRICULTURE FIELDS

ERT Document No. P-A245

FINAL REPORT

December 1980

Prepared for

National Aeronautics & Space Administration
Goddard Space Flight Center
Greenbelt, Maryland 20771

Contract NAS5-25529

Prepared by

Hsiao-hua K. Burke

Environmental Research & Technology, Inc.
696 Virginia Road
Concord, Massachusetts 01742

TABLE OF CONTENTS

ABSTRACT

During the course of this study, three tasks related to soil moisture sensing at microwave wavelengths have been undertaken: (1) Analysis of data at L, X and K_{21} band wavelengths over bare and vegetated fields from the 1975 NASA sponsored flight experiment over Phoenix, Arizona, (2) modeling of vegetation canopy at microwave wavelengths taking into consideration both absorption and volume scattering effects, and (3) investigation of overall atmospheric effects at microwave wavelengths that can affect soil moisture retrieval.

Data for both bare and vegetated fields are found to agree well with theoretical estimates. It is observed that the retrieval of surface and near surface soil moisture information is feasible through multi-spectral and multi-temporal analysis. It is also established that at long wavelengths, which are optimal for surface sensing, atmospheric effects are generally minimal. At shorter wavelengths, which are optimal for atmospheric retrieval, the background surface properties are also established.

1. INTRODUCTION

The feasibility of monitoring soil moisture utilizing passive microwave sensors has been tested through various truck-mount, airborne and space programs. At microwave frequencies the dielectric coefficient of dry soils is much less than that of water. As moisture is added to the soil, the dielectric coefficient increases. The thermal emissions of material are inversely related to their dielectric coefficients. Thus, the brightness temperature, defined as the apparent temperature measured by an antenna assuming that the emitting surface is that of a black body, is much lower for a moist soil than that of a dry soil at the same physical temperature. From a space platform the use of microwaves has the advantage over more conventional techniques that observations can be made at night and through cloud cover. Also, because of the relatively large skin depths of microwave radiation emitted from soils, there is a possibility of detecting the nearsurface water tables.

There are some interrelated problems that must be solved in order to interpret measured signals correctly. These problems concern: (1) the physical significance of the signal emitted by a soil surface as a function of moisture content, (2) the surface roughness conditions that affect the signature, (3) the effect of vegetation medium on the soil moisture retrieval, and (4) the modification of the surface signal by the intervening atmosphere. A multi-layer incoherent radiative transfer model was developed by Burke et al. (1979) to analyze the 1974 aircraft experiment conducted by NASA in Phoenix, Arizona (Schmugge et al. 1976). The model was also compared with others and proved to be applicable and sufficent for a broad range of soil moisture conditions (Schmugge and Choudhury, 1980) The surface roughness effect was recently treated by Choudhury et al. (1979) by using a simple correction factor. It provides sufficient roughness correction at individual wavelengths for various observed data. One shortcoming of the model is that there is a $1/\lambda^2$ dependence in the formulation of the correction factor; such dependence was not observed. The combined Burke et al. model (1979) for soil moisture (Appendix A) and the Choudhury et al. model (1979) for roughness correction are used extensively in this study for the analysis of data taken during a NASA conducted soil moisture experiment in 1975. Measurements of microwave

emissions at 21, 2.8, 1.67, 1.37 and 0.8 cm were made over furrowed bare fields as well as fields with various vegetation canopies. The surface temperature of the soil was monitored using a thermal infrared sensor. These instruments were carried aboard a NASA aircraft flying at an altitude of 500 - 800 meters over agricultural fields near Phoenix, Arizona. Extensive ground truth samples, in the form of moisture and temperature profiles were collected at the time of the aircraft over-passes. Section 2 summarizes the results of data analysis for both bare and vegetated fields.

A comprehensive model for vegetation is presented in Section 3. Two perspectives are taken into account, modeling of dielectric coefficient for the vegetation medium and its volume scattering effect. The model predictions are then compared with data. In Section 4, atmospheric effects on soil moisture retrieval in the microwave region are summarized. Conclusions for this study are presented in Section 5.

2. DATA ANALYSIS OF 1975 FLIGHT DATA

2.1 Summary of the Experiment

During March 1975, an aircraft mission consisting of four flights over the Phoenix, Arizona test site was conducted for the purpose of studying the use of microwave radiometers for the remote sensing of soil moisture. The investigators involved in this mission came from NASA, the Agricultural Research Service of USDA, the University of Arkansas, and Texas A&M University. This mission consisted of predawn and midday flights on 18 and 22 March 1975. There were radiometers operating in the wavelength range 0.8 to 21 cm. The 2.8 cm radiometer is a dual-polarized conically scanning radiometer operating at a fixed look angle of 50°. The other radiometers which were sensitive to emissions at wavelengths of 21, 2.8, 1.67, 1.3 and 0.8 cm were non-scanning but could have their nadir look angles varied. In addition to the microwave instruments the scientific package included a non-scanning infrared radiometer (10-12 μm) for measuring surface temperature. Three passes were taken over each field; one at a nadir angle of $\Theta = 0°$ and two at a nadir angle of $\Theta = 40°$ alternating the polarization sensitivity of the antenna. The aircraft altitude for the $\Theta = 0°$ pass was 800 m and for the $\Theta = 40°$ passes was 500 m.

Ground measurements were made in 46 fields. Twenty-eight were without vegetative cover and 18 had vegetative covers of either alfalfa or wheat. The fields, which have an area of 16.2 hectares (400 x 400 m), were arranged in pairs to provide a uniform target 800 meters wide. The soil moisture sampling procedures for this mission included measurements of the moisture content and temperature in each of the following soil layers: 0-1 cm, 1-2 cm, 2-5 cm, 5-9 cm, and 9-15 cm. The results included data from a variety of moisture conditions due to the irrigation and drying cycles of the fields (Schmugge, 1976).

The data analysis was carried out for 21 cm, 2.8 cm and 1.67 cm measurements. Data from 1.3 cm and 0.8 cm are not presented. An initial investigation showed that brightness temperatures at the shorter wavelengths are relatively insensitive to soil moisture content. Responses to both bare and vegetated fields were studied for nadir and polarized conditions.

In Section 2.2, general analysis of the data are presented and compared with model predictions. In Section 2.3, two Stokes Parameters, $P = \frac{1}{2}(T_{BV} + T_{BH})$ and $Q = (T_{BV} - T_{BH})$, where T_{BV} and T_{BH} are brightness temperatures of the vertical and horizontal polarizations respectively, are analyzed for optimal soil moisture sensing. In Section 2.4, the data are analyzed from different perspectives for possible retrieval of subsurface moisture information.

2.2 General Analyses of Data

21 cm

Nadir and polarized responses at 21 cm for predawn (AM) and mid-afternoon (PM) flights are shown in Figures 2-1 to 2-3. Average soil moisture contents by weight in the top 2 cm are used. For bare fields the correlation between soil moisture up to 20-25% and emissivity is high. For those fields with moisture content greater than 25%, the responses seem to be more variable. An explanation for this is that the surface roughness effect is more pronounced for moist fields. For example, using the estimation method developed by Choudhury et al. (1979), the difference in observed brightntess temperatures between medium rough ($h = 0.3$) and rough ($h = 0.6$) fields is only 6°K for dry fields (SM = 0%) but ∿27°K for wet fields (SM = 25%). In general, data for bare fields agree well with theoretical values with an average roughness factor of $h = 0.5$.

For vegetated fields, the response at nadir and horizontal polarization are similar. The sensitivity to soil moisture information is still strong. The general trend is that for drier fields there is a slight decrease in brightness response due to the vegetation as compared to bare fields. For moist fields, the vegetation canopy produces an increase in brightness temperature of about 15°K. The general increase in brightness temperature can be explained by the vegetation canopy acting as an additional thermal emitting layer. The increase is more for wetter fields due to their lower surface emissivities (higher surface reflectivity). The increase in signature due to vegetation is further compensated by the smoother surfaces under the vegetation relative to the furrow-irrigated bare fields which would produce overall lower

emissivities. As a result, for dryer fields the brightness temperature responses over vegetated fields are similar to, or in some cases lower than, those over bare fields. For vertical polarization, the vegetation effect is more pronounced such that the response is less sensitive to the background soil moisture content. The vegetation model will be discussed in more detail in Section 4.

2.8 cm

The 2.8 cm data are presented in Figures 2-4 to 2-7. There are both vertically and horizontally polarized data at look angle of 50°. Three measurements were taken for each observation. The presented values are averages of the three measurements. In general, the correlation of brightness temperatures to surface moisture content in the top 2 cm for bare fields is better than that at 21 cm. This is due to the fact that at 2.8 cm, radiation comes mainly from the surface while at 21 cm, radiation from both surface and subsurface contribute to the total observed brightness temperature. Typically, the sensitivity of the brightness temperature variation to soil moisture content is about 1.5°K/% moisture change for data from the horizontal polarization and less than 1°K/% moisture change for data from the vertical polarization. Data for bare fields also agree well with theoretical prediction with a roughness factor (h) ranging from 0.3 to 0.5.

Data for vegetated fields, on the other hand, show no correlation to the background soil moisture. The average emissivity for the vegetation canopy at the vertical polarization is .92 and that at the horizontal polarization is .89, both with a small variation of ±.02. Emissivity is defined as the ratio of the brightness temperature to the physical temperature using the IR observation and assuming an isothermal layer between the surface and vegetation. The difference between the two polarizations ($\sim$0.03 - 0.04) can be attributed to the attenuated surface background which in absence of vegetation would produce a difference in emissivities of .07 to .1 between signatures from two polarizations. The observed vegetation response also agrees in general with the vegetation model presented in Section 4. In general, the vegetation canopy becomes "opaque" at this wavelength. Furthermore, brightness temperature is generally 20°-30°K lower than the physical temperature, a phenomenon that can be attributed to the scattering effect of the vegetation layer.

1.67 cm

Data of 1.67 cm were analyzed in the same fashion as those of 21 cm and 2.8 cm. They are shown in Figures 2-8 to 2-10 for nadir, horizontally and vertically polarized observations respectively. The look angle for polarized observations was 40°. In general, the correlation of brightness temperatures to surface moisture for bare fields is similar to that at 2.8 cm. Radiation at this wavelength is mainly from the surface layer. Sensitivity of the brightness temperature to the surface soil moisture variation is about 1.5°K/% moisture change for observation from horizontal observation and less than 1°K and about 1°K for those from vertical and nadir observations respectively.

Data for vegetated fields also do not show correlation to the background soil moisture conditions. The average emissivity for the vegetation canopy at the vertical polarization is .90 and that at the horizontal polarization is .86. The difference between two polarizations is similar to that at 2.8 cm. The overall lower emissivity of vegetation than that at 2.8 cm is resultant of the stronger scattering effect at 1.67 cm than 2.8 cm due to the inverse wavelength dependence of the scattering effect which will also be discussed in Section 4.

2.3 Polarization Effects on Soil Moisture Conditions

The polarization information from soil moisture measurements was first investigated by Burke and Paris (1975) on the 1974 Phoenix data. Two of the Stokes parameters $P = \frac{1}{2}(T_V + T_H)$ and $Q = (T_V - T_H)$, where T_V and T_H are brightness temperatures from the vertical and horizontal polarizations respectively, were studied to determine the polarization effects. It was shown that P is relatively insensitive to the surface roughness characteristics. Furthermore, it was also predicted that Q, which increases as moisture content increases, should be another useful parameter. The broad moisture range of the 1975 set of Phoenix data enabled a closer look of these effects.

Figures 2-11a and b demonstrate the response of $\frac{1}{2}(T_V + T_H)$ versus nadir brightness temperature at 21 cm and soil moisture content respectively. As can be seen from Figure 2-11a, the nadir brightness temperature and $\frac{1}{2}(T_V + T_H)$ are always close to each other. This is significant

because it implies that in a scanning system, P may be independent of angle and thus provides an easy means of analyzing data. It is also shown in Figure 2-11b that the scatter of the $\frac{1}{2}(T_V + T_H)$ data as a function of soil moisture content is less than that of either the vertical or horizontal polarization. This further demonstrates the feasibility of utilizing P as a practical parameter for soil moisture retrieval.

Figure 2-12 shows responses of $Q = (T_V - T_H)$ versus soil moisture content at 21 cm for both bare and vegetated fields. Although there is a correlation between Q and soil moisture content, the scatter is too big for this parameter to be useful for soil moisture retrieval. However, Q may be an indicator of surface roughness. As can be seen, Q is larger for vegetated fields; this is due to the smoother surfaces that were present under the vegetation canopy. These vegetated fields were not furrow-irrigated as the bare fields. Thus, it is feasible that utilization of the combined P and Q parameters can be quite useful for remotely monitoring soil conditions.

2.4 Possible Retrieval of Subsurface Moisture Information

The subsurface moisture information can be obtained through timely observations during a drying cycle from measurements from different wavelengths. During the 1975 Phoenix experiment, both predawn and afternoon data were collected on two separate days. Many of the fields had been irrigated about a week before the first flight so that subsurface layers of these fields were moist. The second day of the experiment was conducted four days after the first, therefore allowing observation through the drying cycle. The effective emissivities at dawn are plotted as a function of their values the same afternoon at wavelengths of 21 cm and 1.67 cm (Figure 2-13). At 1.67 cm, almost all of the fields have emissivities at dawn that are less than their afternoon values due to the evaporation process during the day. Fields with lower emissivities both at predawn and in the afternoon can be assumed to hold water below the surface. Fields with the highest emissivities, which are also the direst, have the same values at dawn and during the afternoon, indicating that there is little free water available beneath the surface. For 21 cm, most of the radiation comes from deeper in the soil. The measured temperature of the soil at a depth of 15 cm generally ran 5°K

warmer than the surface at dawn and about 10°K cooler during the afternoon. The surface temperatures were generally within 2°K of the 0-1 cm layer value. Therefore, in addition to the moisture condition, emissivity is also affected by the relative change in the physical temperatures. An $\varepsilon_{Dawn} = \varepsilon_{Afternoon} + .05$ line is drawn to roughly allow for subsurface temperature effects. It is seen that for drier fields, the afternoon emissivity is relatively lower due to the change of surface-to-subsurface temperature gradient from predawn to the same afternoon. For fields with moist subsurfaces, the emissivity variation is further dependent upon the surface moisture condition affected by the daytime evapotranspiration processes.

Another way of looking at the same effect is shown in Figure 2-14 where dawn and afternoon emissivities at 1.67 cm and 21 cm are plotted together as a function of the surface moisture content (0-2 cm). Emissivities at 1.67 cm for both dawn and afternoon data all lie close to the same regression line. At 21 cm, the regression line is followed quite well for moistures greater than 15%. For fields with surface moisture less than 15%, the dawn observations lie above the regression line and the afternoon observations below. The magnitude of fluctuations of emissivity from dawn to afternoon can be used as an indicator of the subsurface moisture content. Thus, it is feasible that information of the moisture gradients of soil can be obtained from a time sequence of combined measurements at different wavelengths.

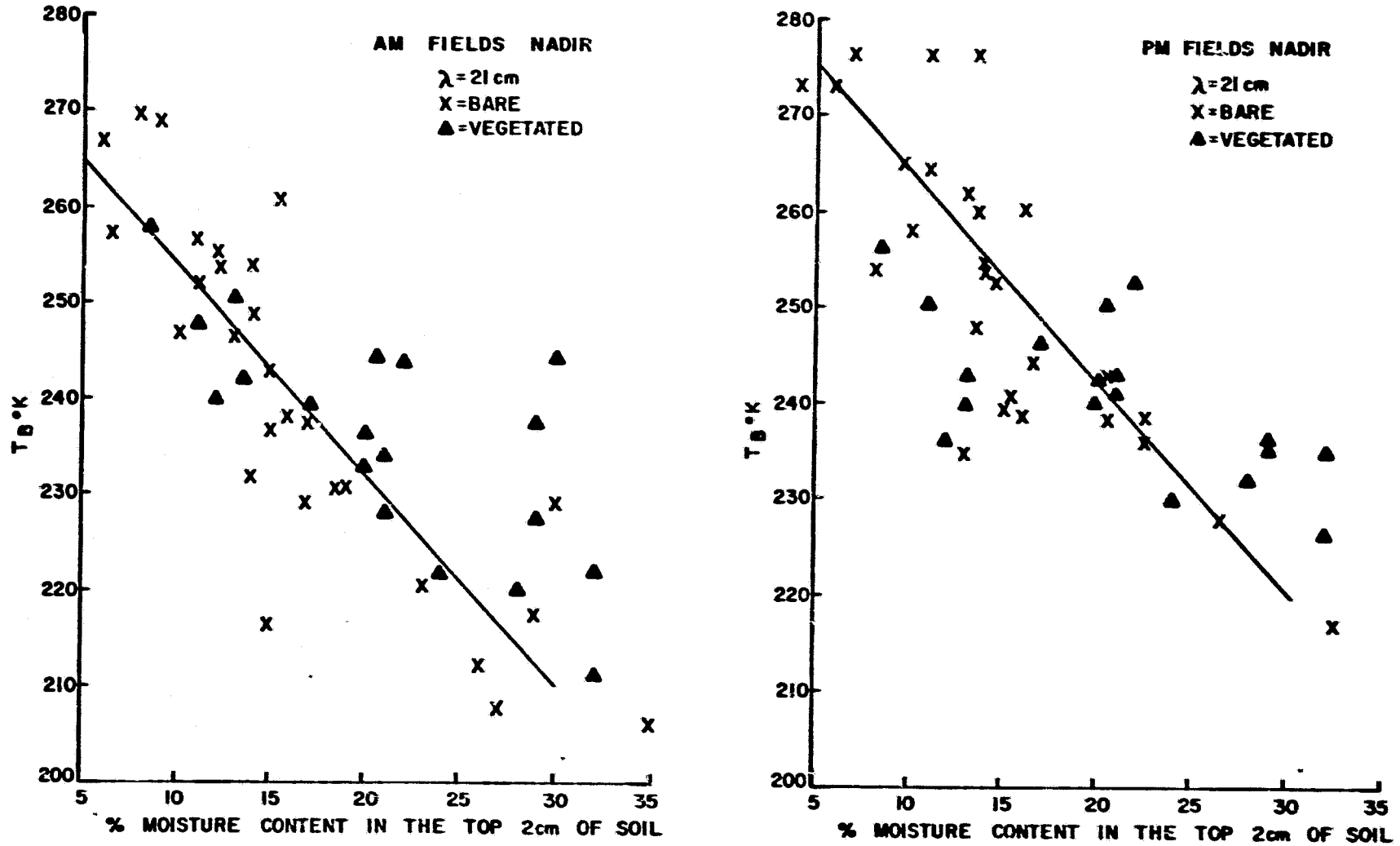

Figure 2-1 Observed nadir brightness temperature on March 18 and 22 (1975 Phoenix Experiment) as a function of average soil moisture content in the top 2 cm layer for λ = 21 cm

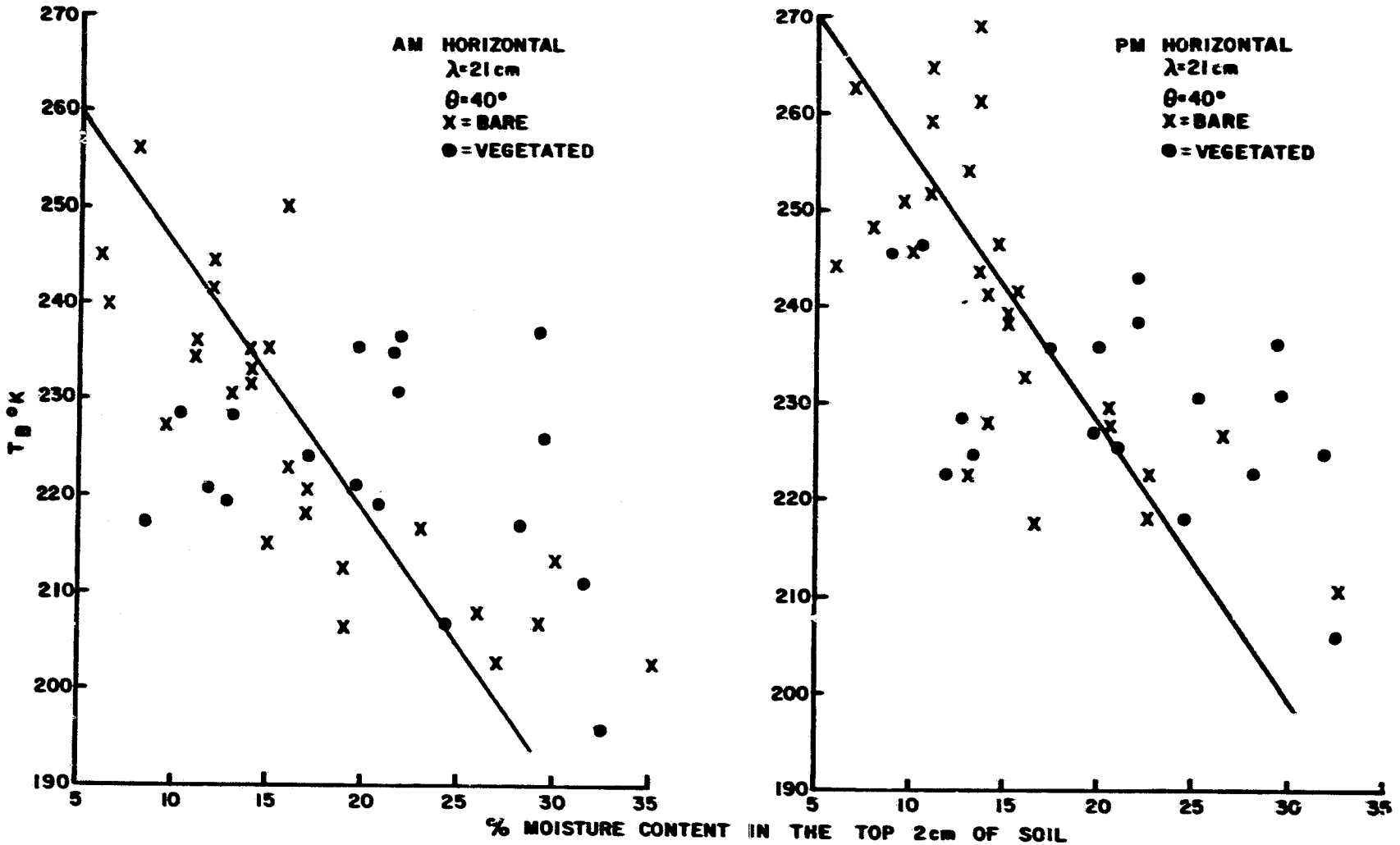

Figure 2-2 Observed brightness temperature of horizontal polarization on March 18 and 22 (1975 Phoenix Experiment) as a function of average soil moisture content in the top 2 cm layer for λ = 21 cm, θ = 40°

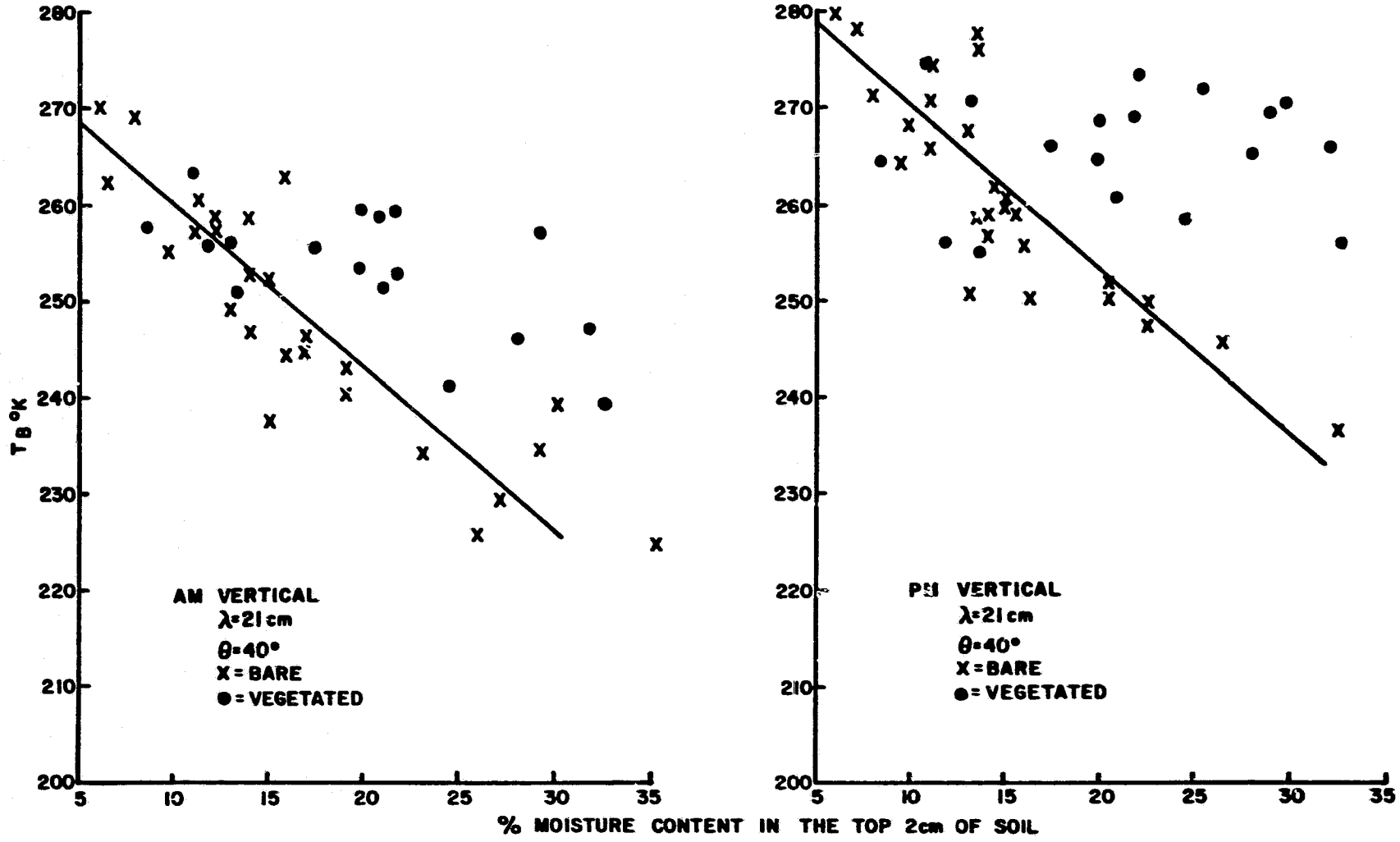

Figure 2-3 Observed brightness temperature of vertical polarization on March 18 and 22 (1975 Phoenix Experiment) as a function of average soil moisture content in the top 2 cm layer for λ = 21 cm, θ = 40°

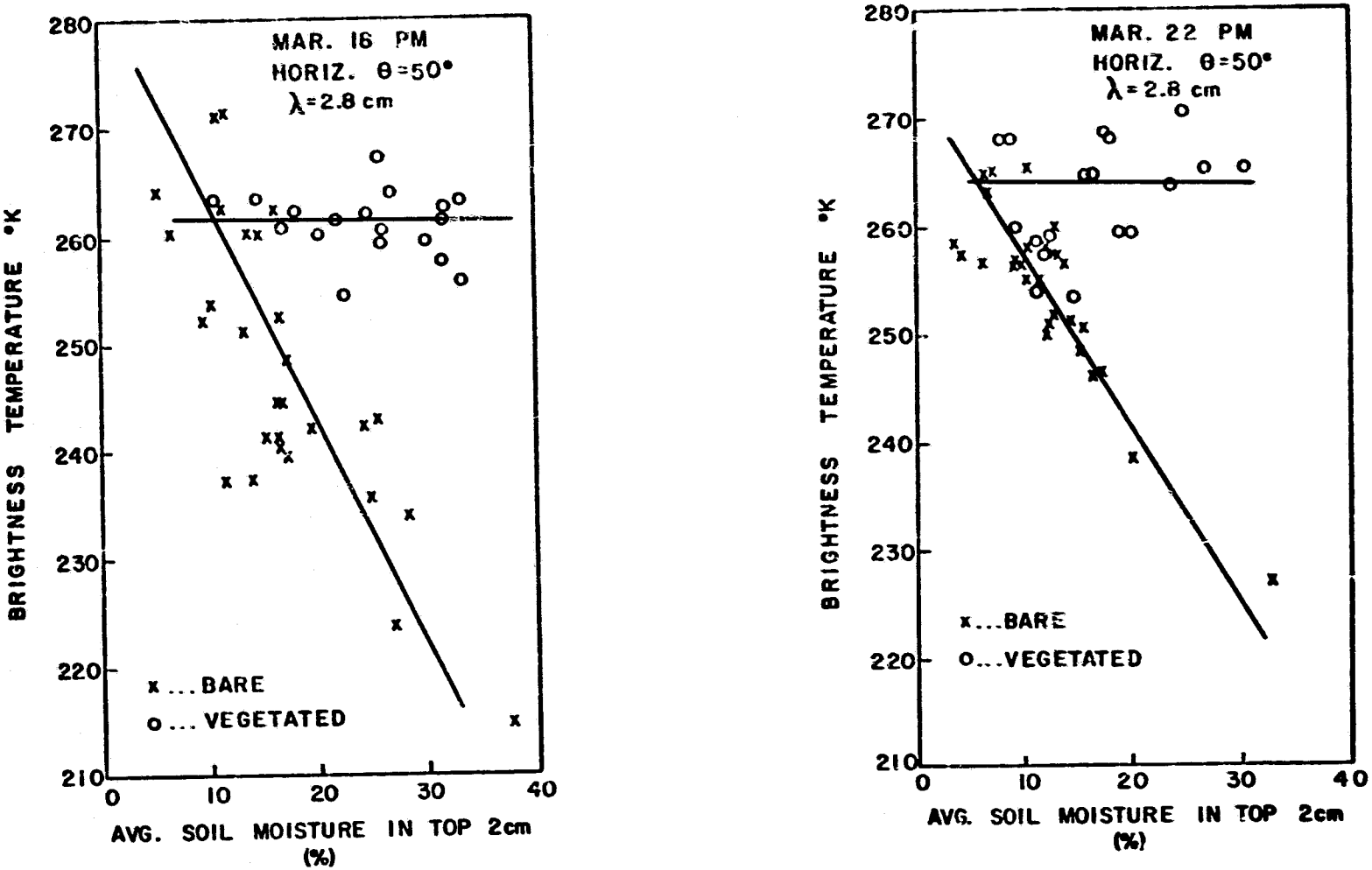

Figure 2-4 Observed horizontal brightness temperature on March 18 and 22 PM (1975 Phoenix Experiment) as a function of average soil moisture content in the top 2 cm layer for λ = 2.8 cm and θ = 50°

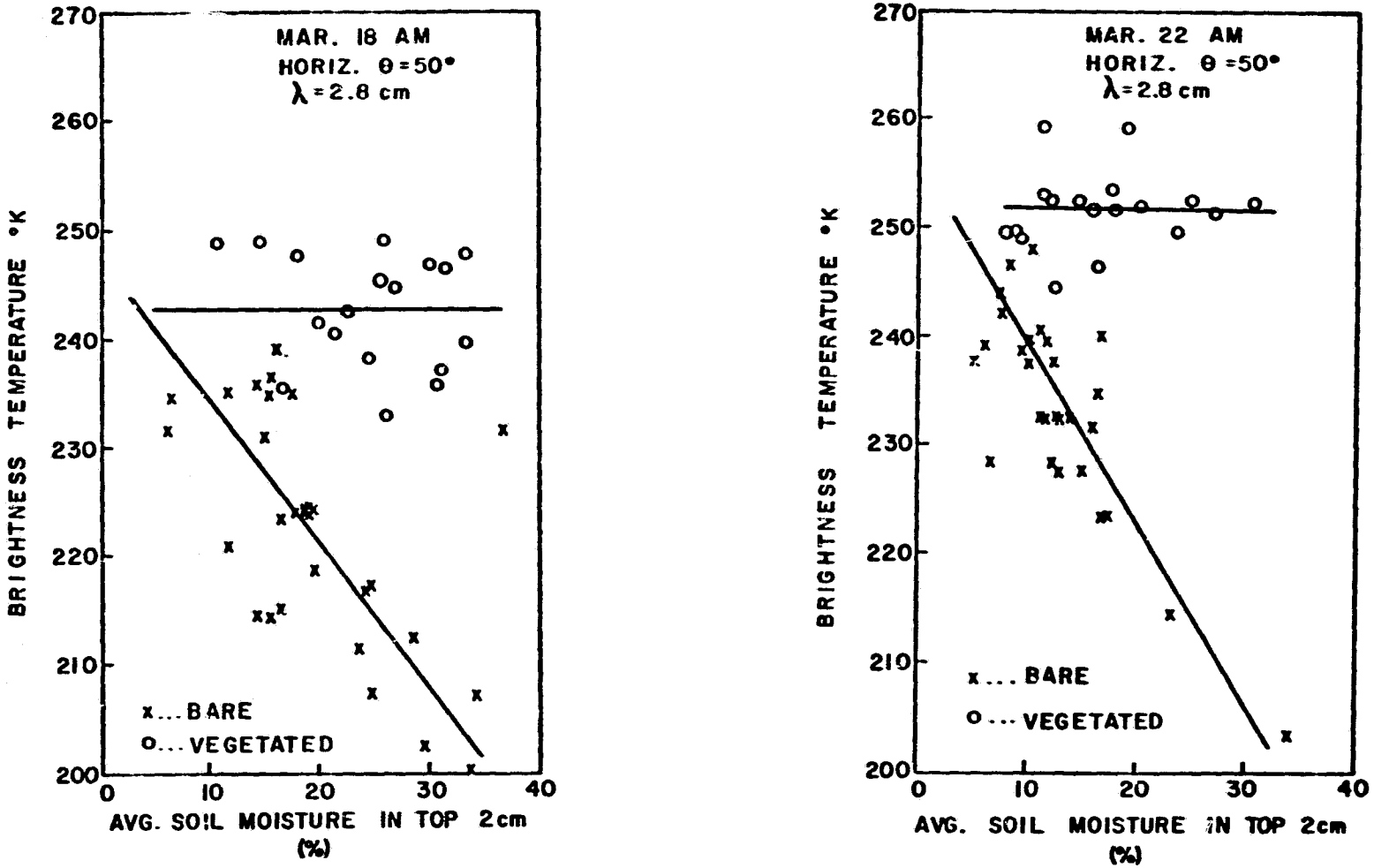

Figure 2-5 Observed horizontal brightness temperature on March 18 and 22 AM (1975 Phoenix Experiment) as a function of average soil moisture content in the top 2 cm layer for λ = 2.8 cm and θ = 50°

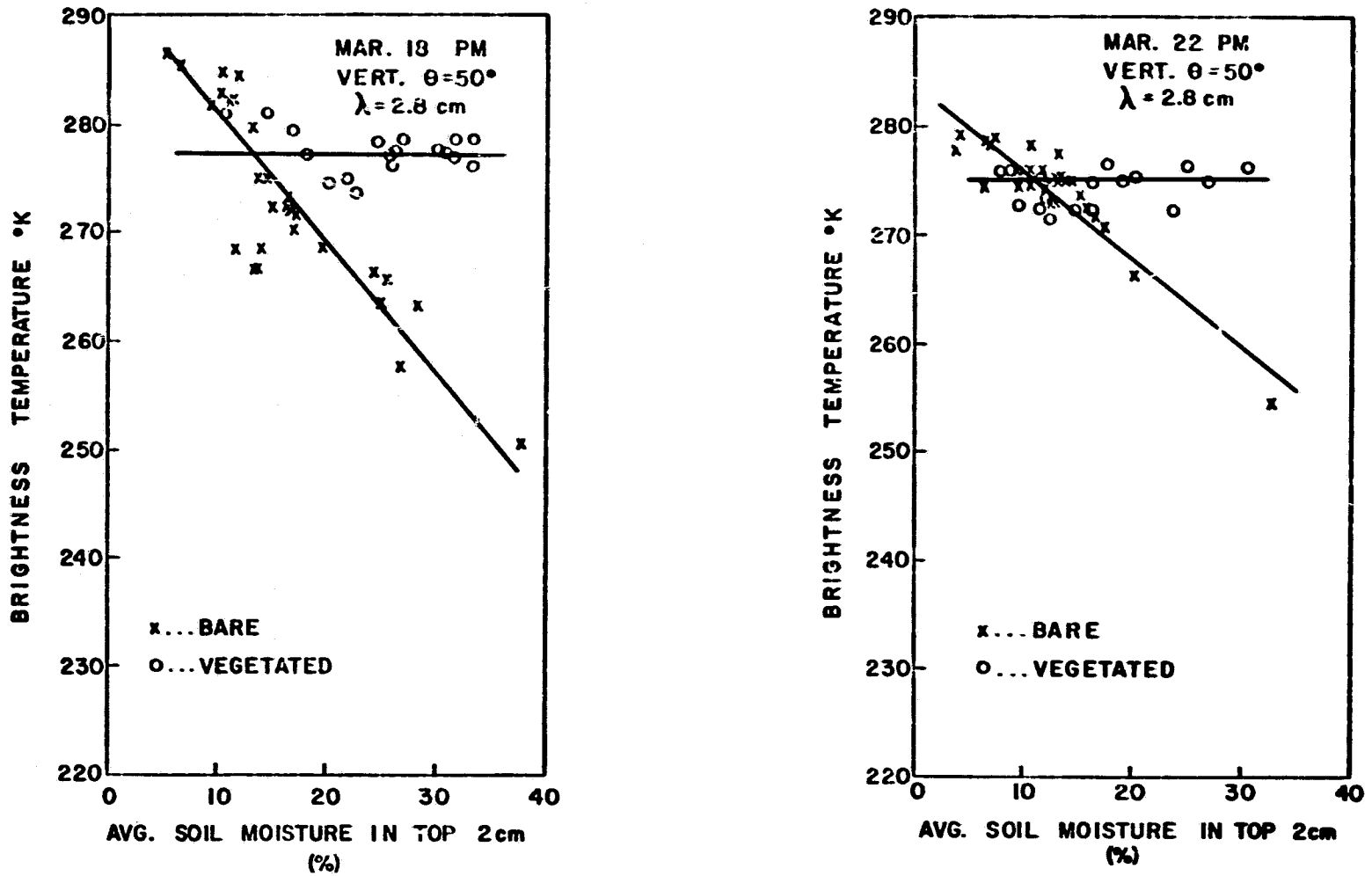

Figure 2-6 Observed vertical brightness temperature on March 18 and 22 PM (1975 Phoenix Experiment) as a function of average soil moisture content in the top 2 cm layer for λ = 2.8 cm and θ = 50°

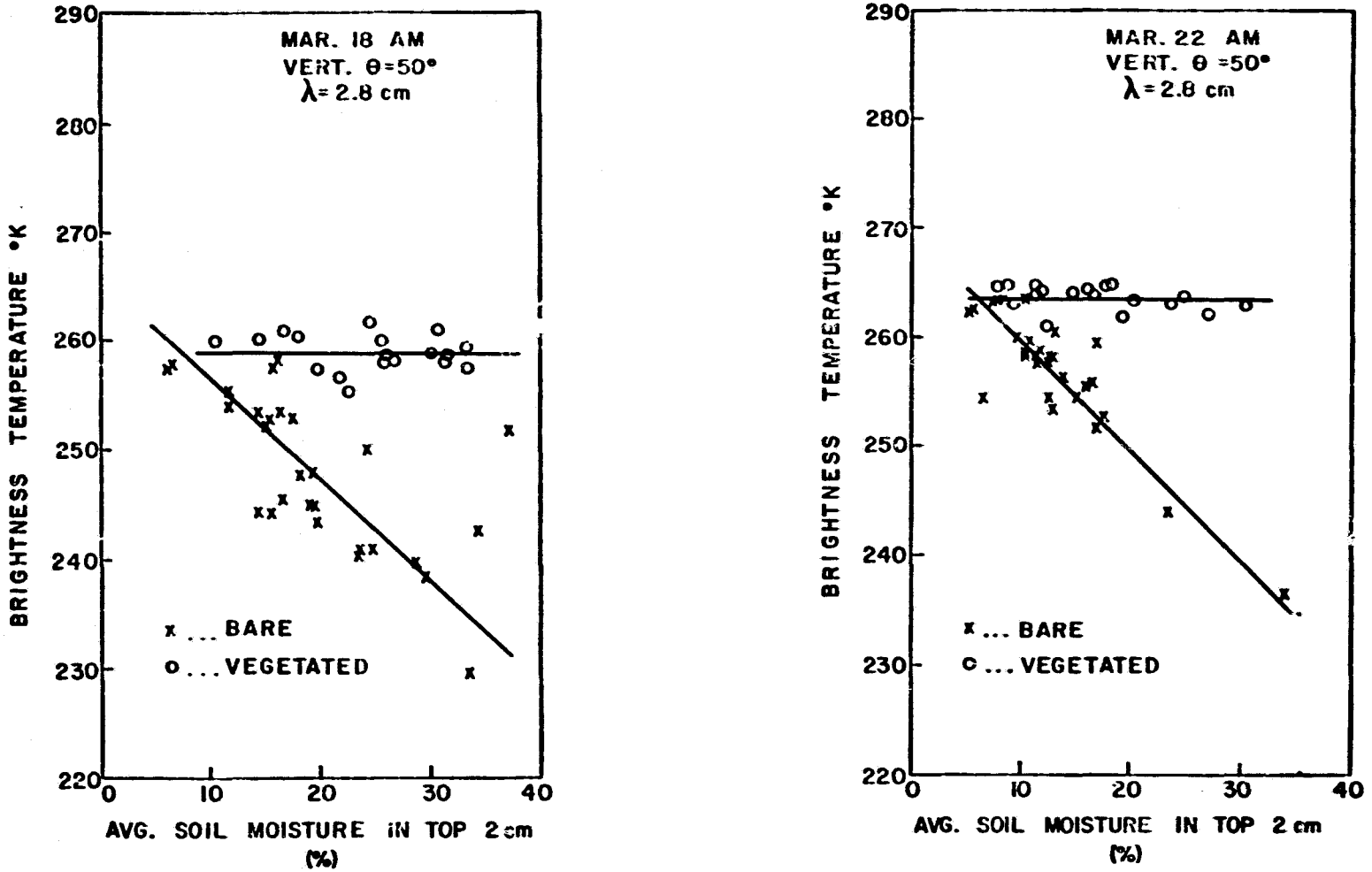

Figure 2-7 Observed vertical brightness temperature on March 18 and 22 AM (1975 Phoenix Experiment) as a function of average soil moisture content in the top 2 cm layer for λ = 2.8 cm and θ = 50°

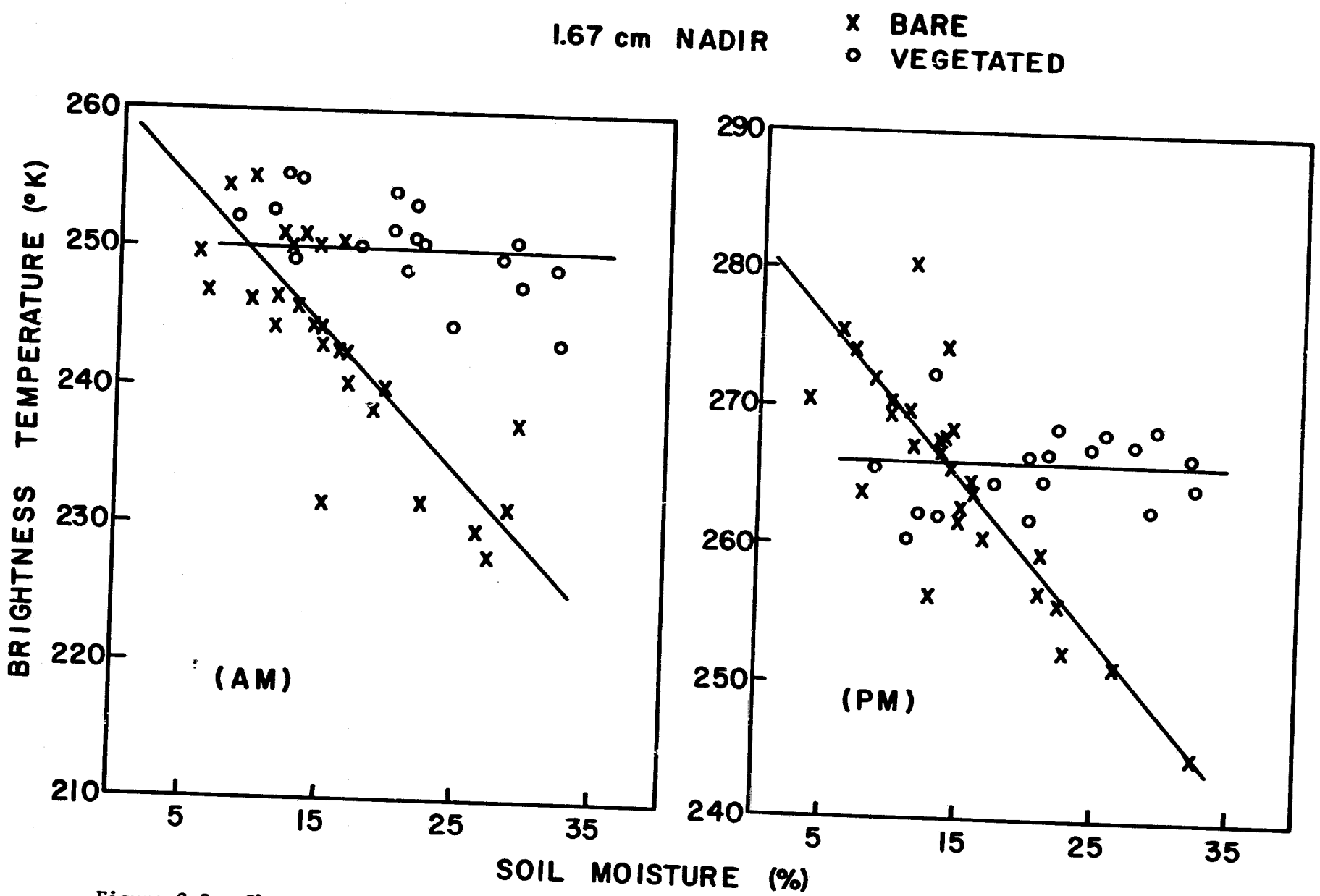

Figure 2-8 Observed nadir brightness temperature on March 18 and 22 (1975 Phoenix Experiment) as a function of average soil moisture content in the top 2 cm layer for λ = 1.67 cm

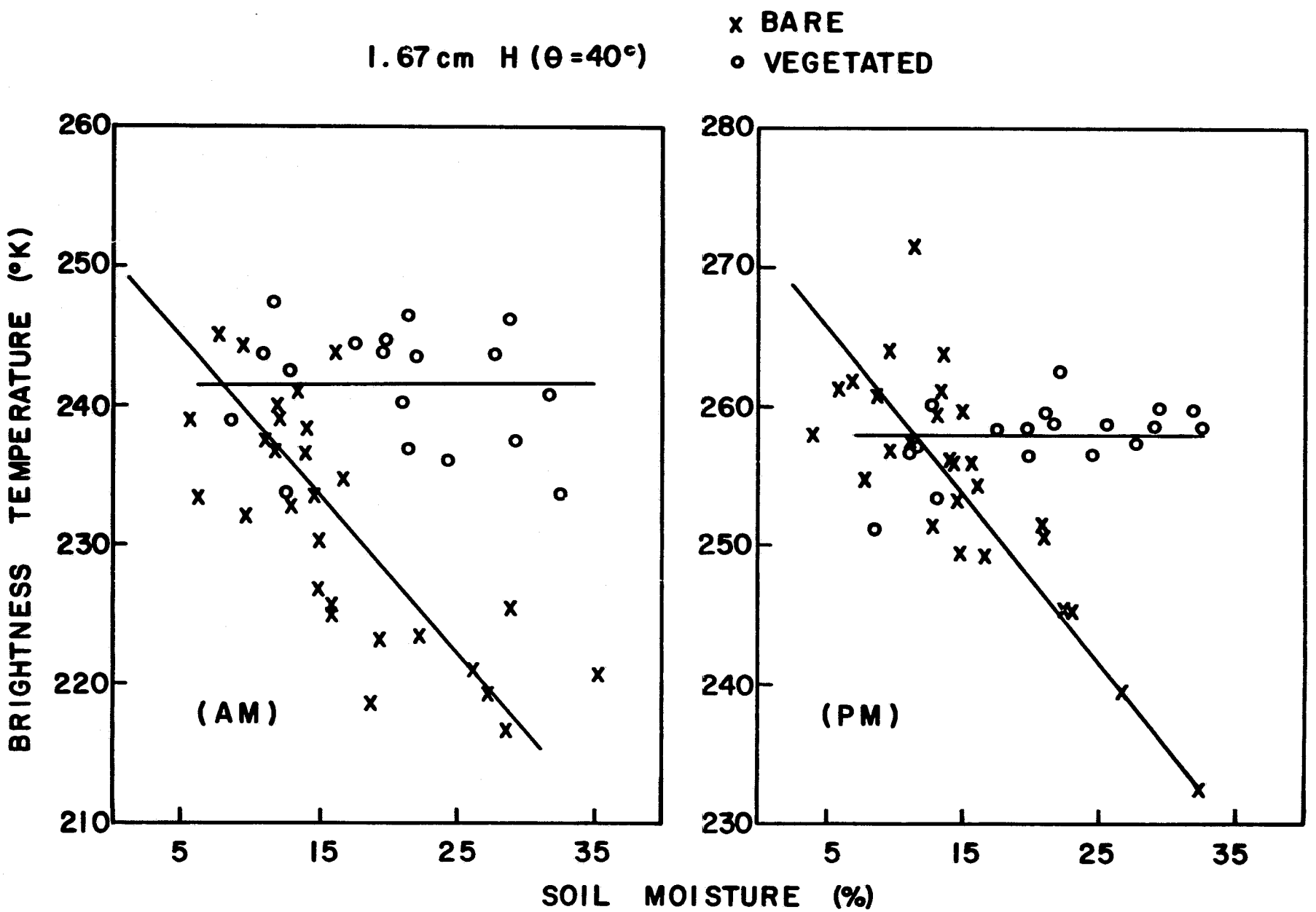

Figure 2-9 Observed horizontal brightness temperature on March 18 and 22 (1975 Phoenix Experiment) as a function of average soil moisture content in the top 2 cm layer for $\theta = 40^{\circ}$

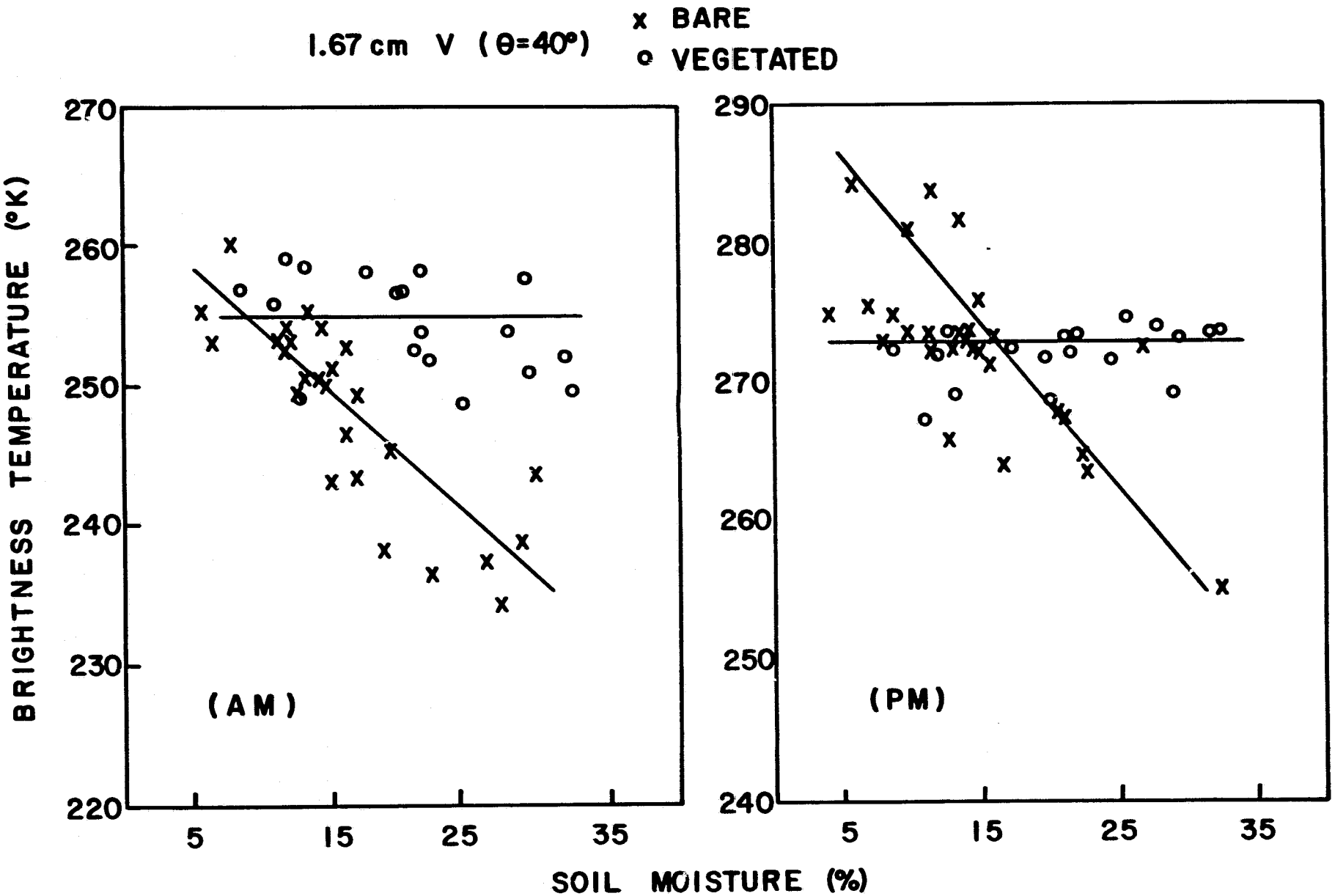

Figure 2-10 Observed vertical brightness temperature on March 18 and 22 (1975 Phoenix Experiment) as a function of average soil moisture content in the top 2 cm layer for $\theta = 40°$

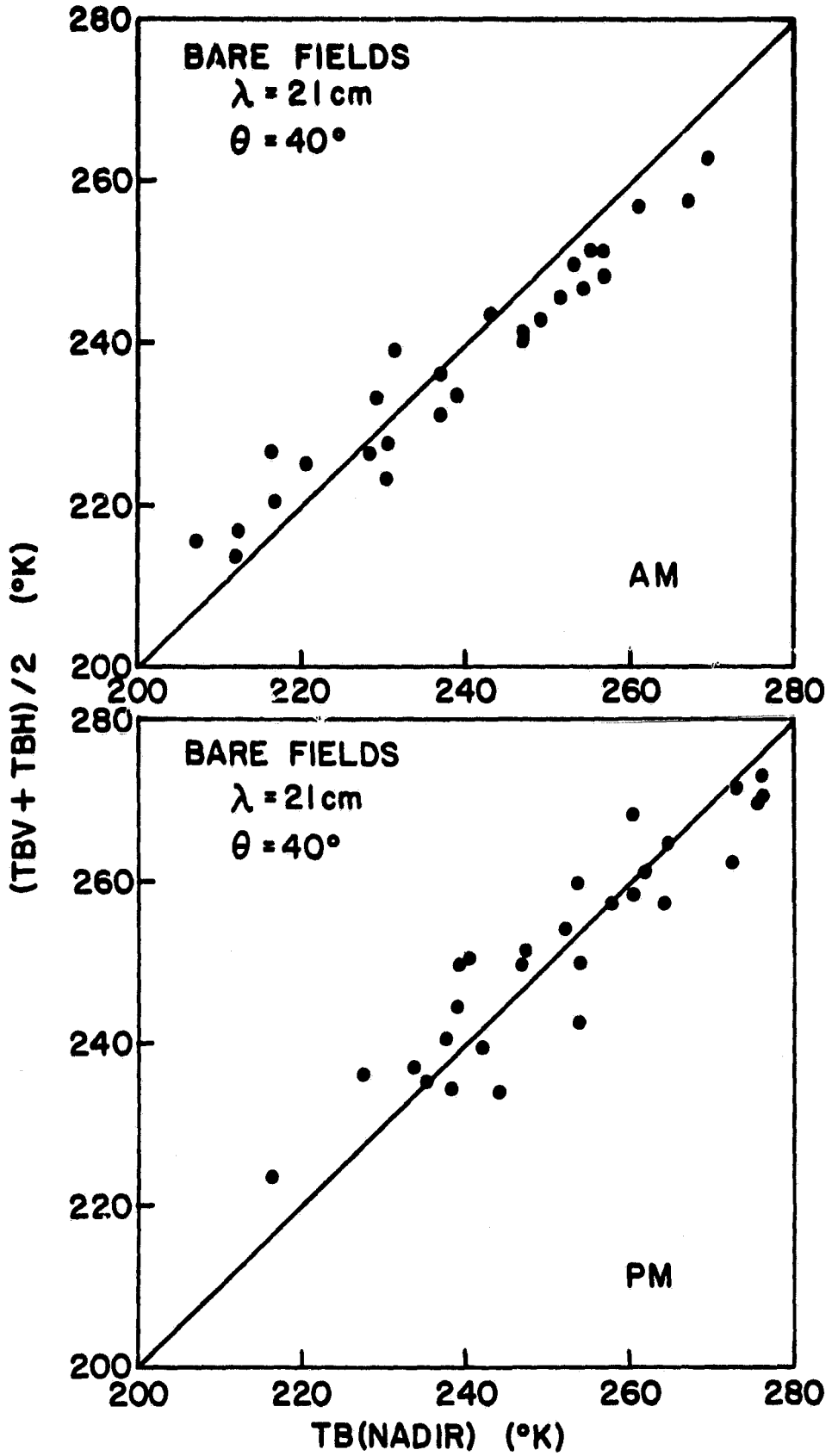

Figure 2-11a The response of $\frac{1}{2}(T_V + T_H)$ at λ = 21 cm, Θ = 40° as a function of the corresponding nadir brightness temperature

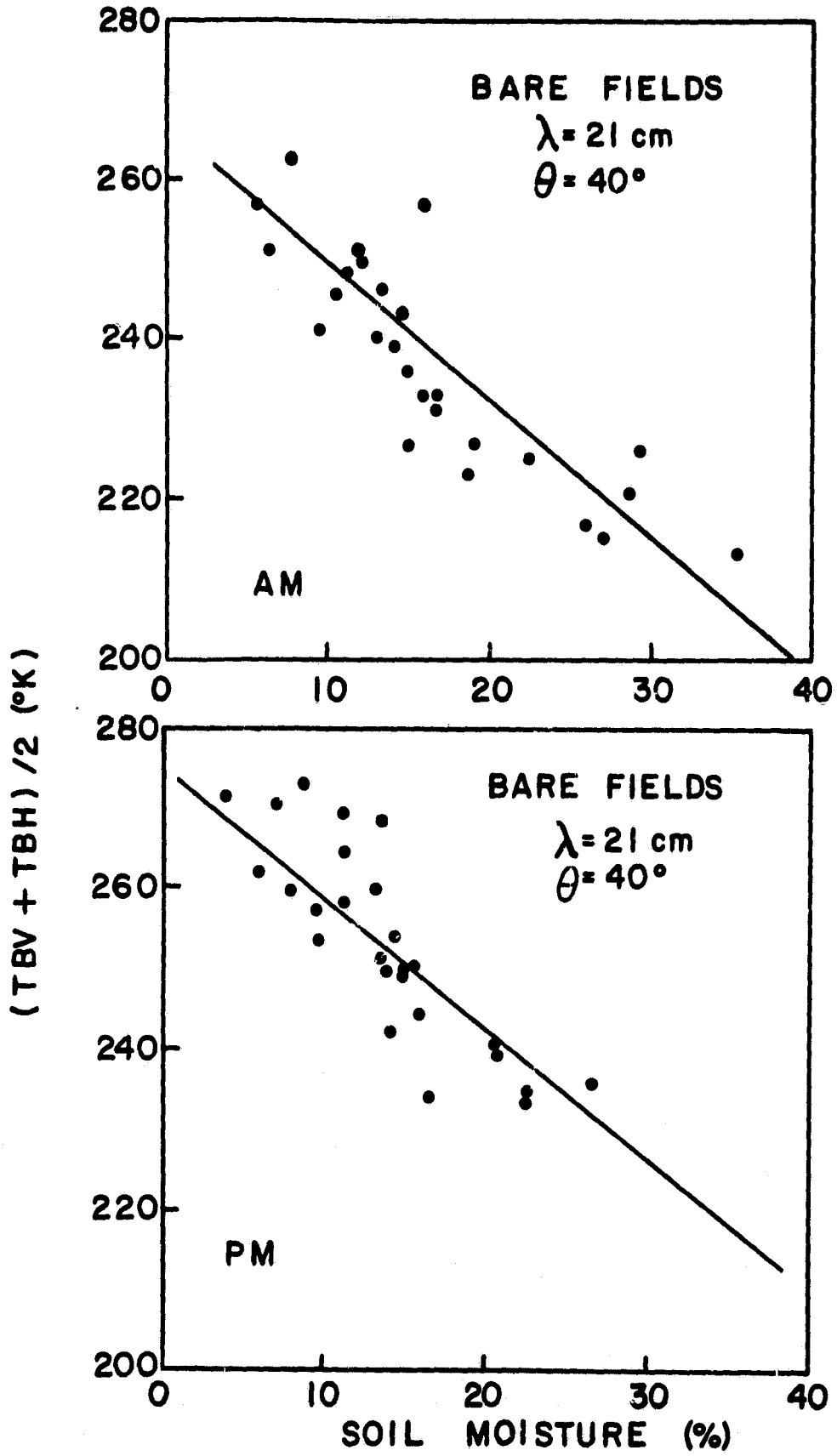

Figure 2-11b The response of $\frac{1}{2}(T_V + T_H)$ at λ = 21 cm, Θ = 40° as a function of soil moisture content in the top 2 cm layer

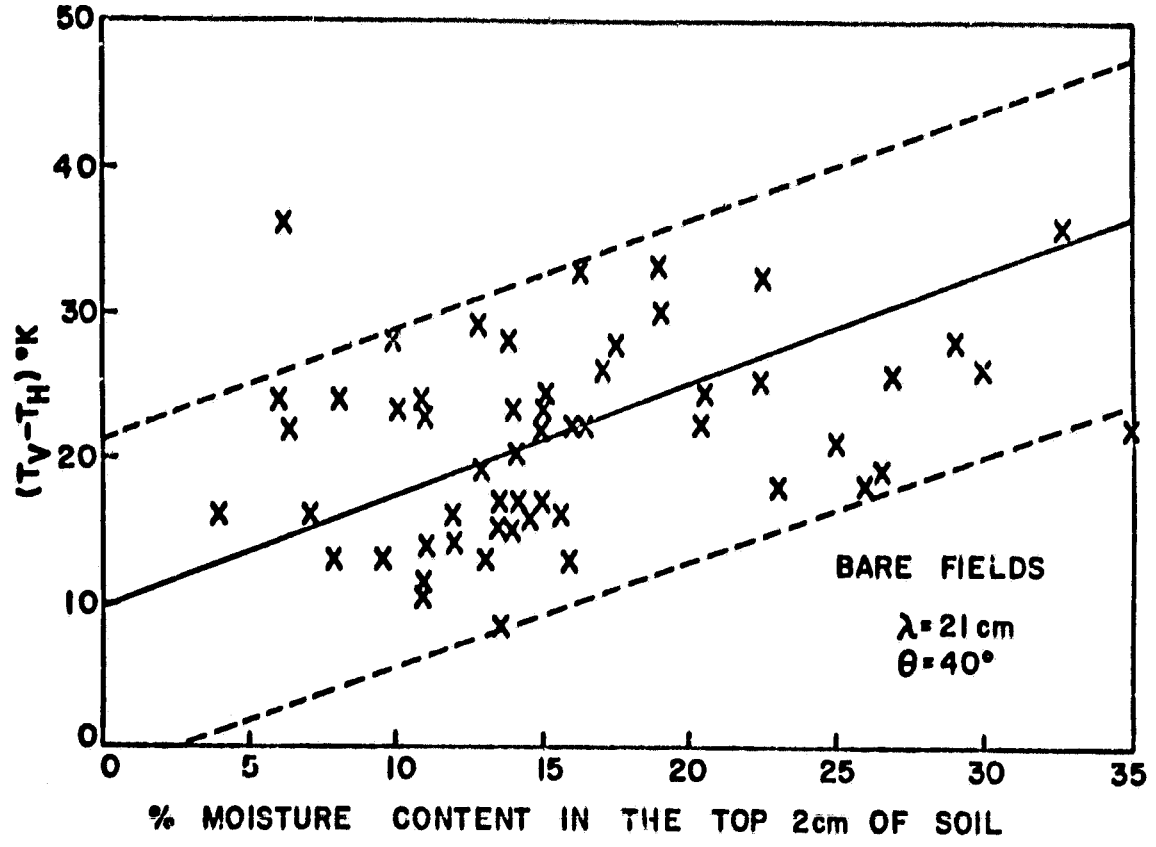

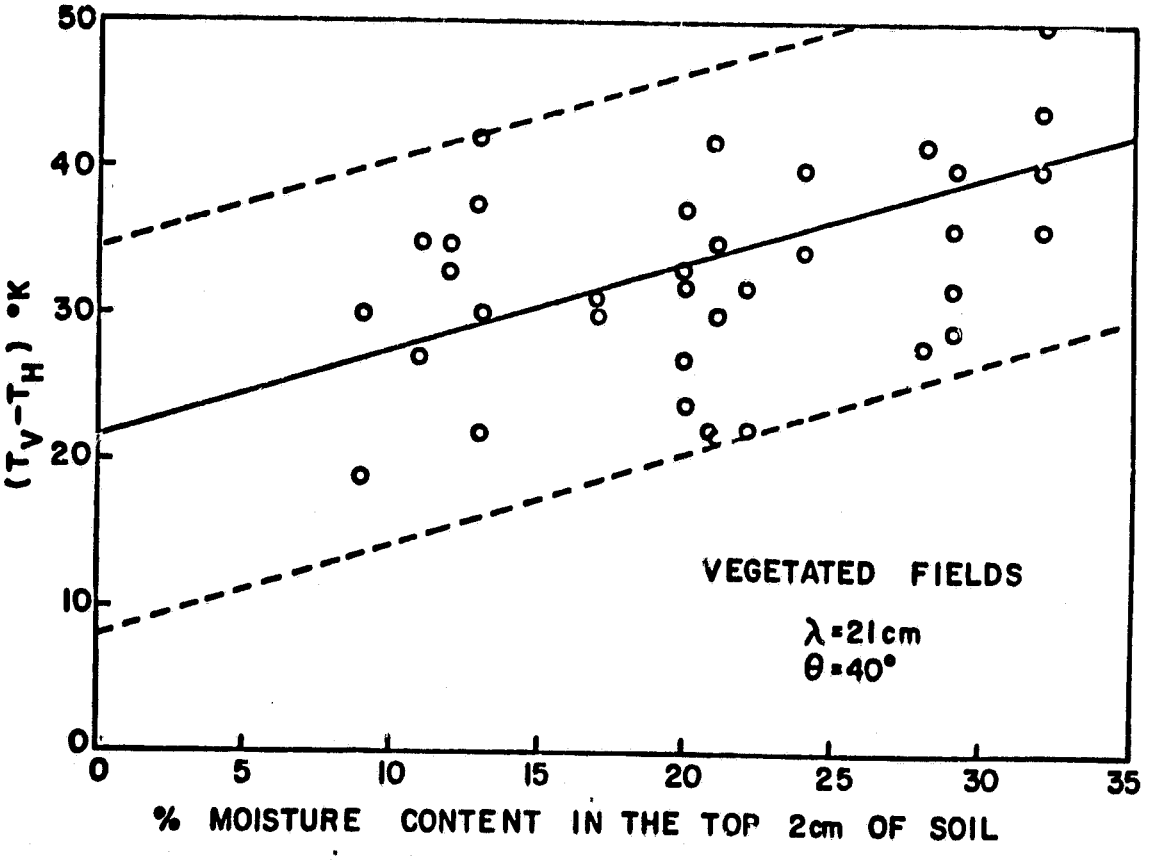

Figure 2-12 The response of $(T_V - T_H)$ at λ = 21 cm, Θ = 40° as a function of soil moisture content in the top 2 cm layer

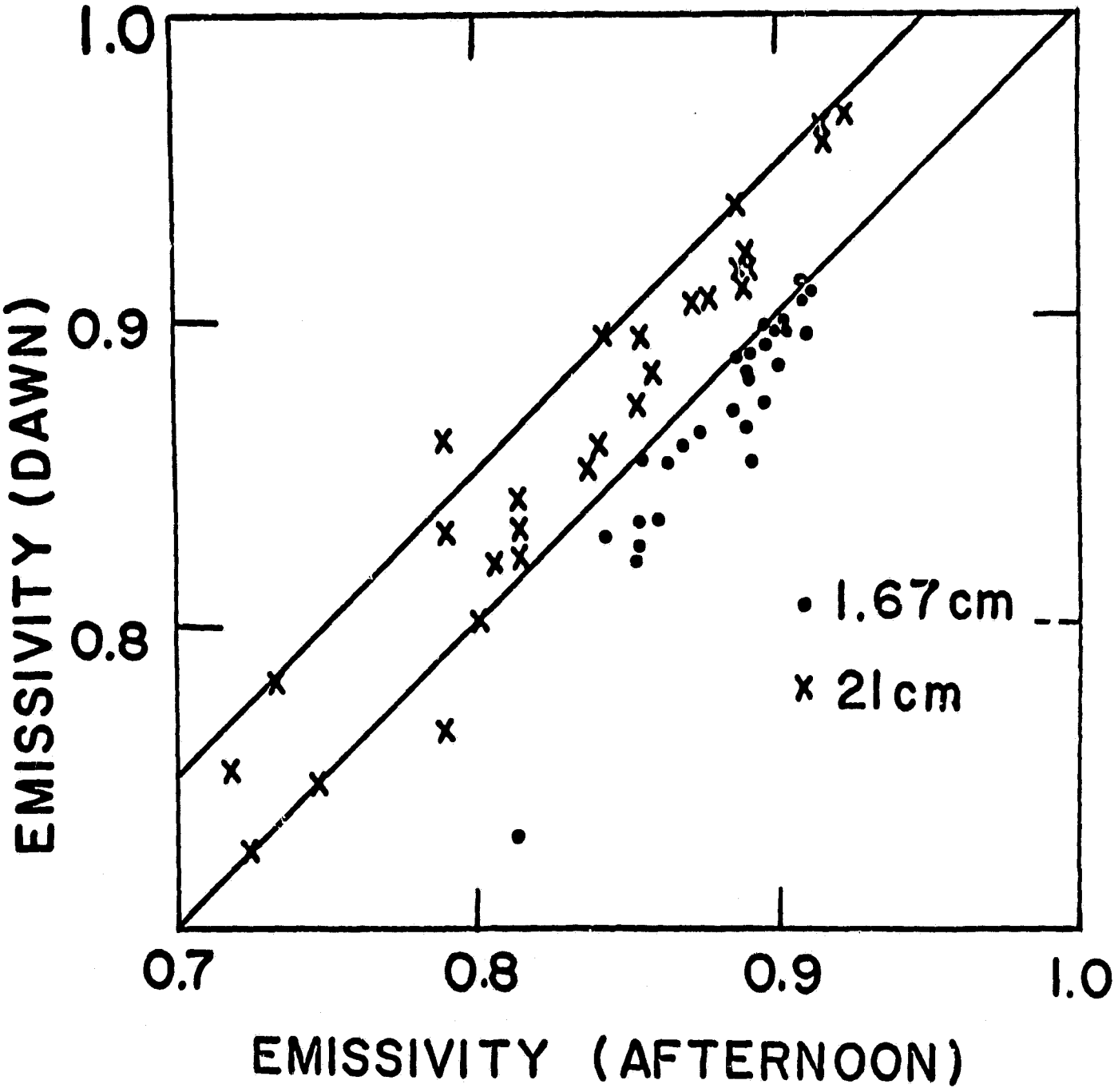

Figure 2-13 Effective emissivities at λ = 1.67 cm and 21 cm at dawn as a function of its value the same afternoon

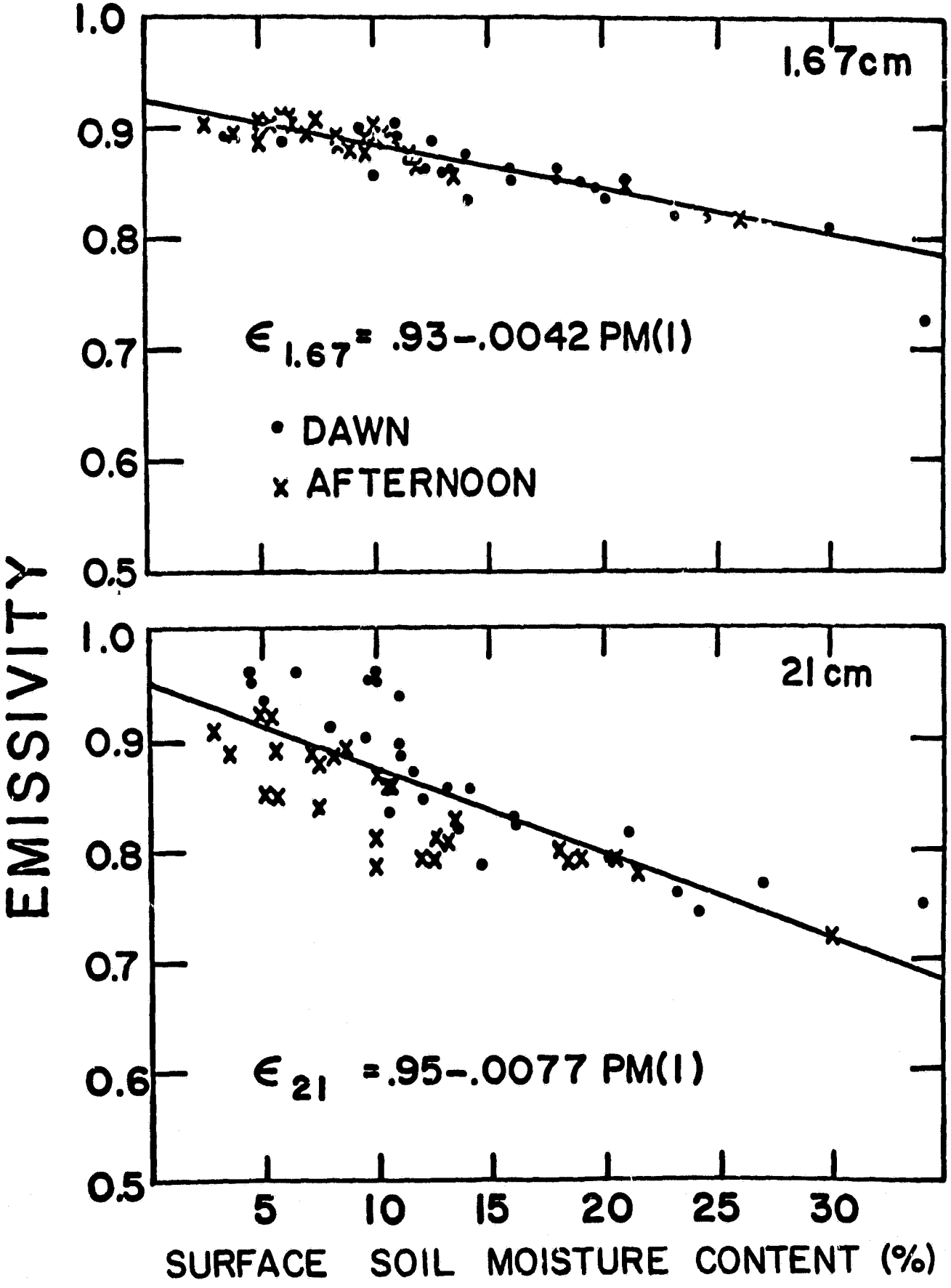

Figure 2-14 Emissivities for λ = 1.67 cm and 21 cm at dawn and afternoon as a function of average soil moisture content in the top 2 cm layer

3. VEGETATION MODEL

3.1 General Characteristics of Vegetation Canopy at Microwave Wavelengths

One major purpose of soil moisture research is to predict and monitor the availability of soil moisture to agriculture application and to assist in the area of crop forecast. At microwave wavelengths, the response of brightness temperature to surface soil moisture of bare fields has been well established. However, once vegetation is present, the signatures are contaminated to various degrees according to the type and coverage of the vegetation, the background condition and the wavelength of observation. Generally speaking, the microwave response observed through a vegetation canopy is as follows:

1) the capability of radiation propagating through a vegetation layer is proportional to the wavelength. At longer wavelengths (L Band), the surface variations can still be observed through a vegetation layer. At shorter wavelengths, the background surface is obscured even with small amounts of vegetation cover;

2) under conditions when surface can be observed through vegetation cover, the higher the background reflectivity (lower emissivity) the more "obscuration effect" of vegetation is expected;

3) the amount of absorption through a vegetation layer is directly proportional to the volume water content of the vegetation. The volume water content is a function of the plant height, density (sparse or cluttered) and condition (dry or wilting). For a forest coverage, the vegetation effect is maximum. Thus, the emissivity can be assumed to be close to one (brightness temperature $\sim$ physical temperature);

4) generally speaking, at longer wavelengths the volume scattering property of a vegetation medium is minimal.

Therefore, an approximation treating the vegetation medium as an additional dielectric slab above the surface is sufficient. This can be applied using the multilayer radiative transfer model developed for soil moisture as shown in Appendix A. The vegetation medium is simply an additional layer with the defined dielectric coefficient. In this approach, dielectric properties play a major role in the microwave response; and

5) at shorter wavelengths, the background surface is obscured in the presence of vegetation. Volume scattering is important and the observed brightness temperature is lower than the physical temperature. Scattering from a vegetation layer is a function of the wavelength and actual structures of the plants. At X and K band wavelengths, a vegetation layer of wheat and alfalfa can produce a cooling effect of 20-30°K due to volume scattering such as observations from the 1975 Phoenix experiment. Similar cooling effect was also observed by Kirdyashev et al. (1979) from fields of winter rye and corn.

In summary, in order to model the vegetation coverage in the microwave range, two models are required along with physical properties of the vegetation canopy: the model of complex dielectric coefficients for vegetation material and the model of volume scattering for the vegetation medium. Modeling for the dielectric coefficient is summarized in Section 3.2 and the volume scattering model is discussed in Section 3.3

3.2 Models of Dielectric Coefficient for Vegetation Medium

There are various ways of theoretically computing, or empirically relating, the dielectric coefficient of vegetation material at different wavelengths. Three representative approaches are summarized here and their impacts studied.

The simplest approach is to assume that vegetation material during growth is mostly water (Attema et al., 1978). Using dielectric

coefficients for water (ε_{water}) and air (ε_{air}), the equivalent complex dielectric coefficient of the vegetation medium (ε_{veg}) is simply a linear combination of the air-vegetation mixture:

$$\varepsilon_{veg} = V_v * (\varepsilon_{water}) + V_a * (\varepsilon_{air}) \tag{3-1}$$

where V_v and V_a are volume fractions of vegetation and air respectively.

The dielectric property of vegetation has also been estimated by Peake (1959) as a function of the fraction of water by weight in the plant (M). The simple assumption is that in the microwave range, the dry vegetated material has a dielectric constant of 2.5. The expression for the vegetated material (ε_v) is thus:

$$\varepsilon_v = M * \varepsilon_{water} + (1 - M) * 2.5 \tag{3-2}$$

and that for the vegetated medium is:

$$\varepsilon_{veg} = V_v * (\varepsilon_v) + V_a * (\varepsilon_{air}) \tag{3-3}$$

Another more comprehensive, and thus more complex, model for dielectric properties of vegetated material was undertaken by de Loor and Meijboom (1966). In their model, the dielectric properties of vegetated material was further developed as a function of both moisture by volume (V_w) and moisture by weight (M). The expressions are:

$$\begin{aligned} \varepsilon_v(\text{Real}) &= 5.5 + (\varepsilon_m - 5.5)/(1 + f^2\tau^2) \\ \varepsilon_v(\text{Im}) &= (\varepsilon_m - 5.5) * f\tau/(1 + f^2\tau^2) \end{aligned} \tag{3-4}$$

where $f\tau$ is approximately $1.85/\lambda$ (λ in cm) in the microwave region and

$$\varepsilon_m = 5 + 51.5 * V_w \tag{3-5}$$

V_w is further related to M by the densities of the solid material (ds) and the density of water (dw) as

$$M = V_w/[V_w + (1 - V_w)(ds/dw)] \tag{3-6}$$

The dielectric coefficient for the vegetated medium is then derived by equation (3-3).

Table 3-1 lists dielectric coefficients at λ = 20 cm and 3 cm derived from the three approaches. Assumptions are that the volume density of vegetation is 1%, moisture fraction by weight of the plant (M) is 0.8 and the density of the solid material is such that dw/ds = 4.

TABLE 3-1

COMPLEX DIELECTRIC COEFFICIENTS OF VEGETATION MEDIUM AT λ = 20 AND 3 CM

Approach	Wavelength	
	20 cm	3 cm
1. Direct	(1.8, .05)	(1.64, .30)
2. Peake	(1.64, .04)	(1.49, .24)
3. de Loor and Meijboom	(1.30, .022)	(1.23, .12)

In order to show the effect of dielectric coefficient of the vegetation layer, the approximation of treating the vegetation medium as an additional dielectric slab is used. With the same assumptions for Table 3-1 and a vegetation layer thickness of 15 cm and background soil moisture content of 15%, the brightness temperature responses from three dielectric models are summarized in Table 3-2.

TABLE 3-2

BRIGHTNESS TEMPERATURES EXPECTED AT λ = 20 CM AND 3 CM USING DIELECTRIC SLAB APPROACH WITH THREE DIFFERENT DIELECTRIC MODELS

Dielectric Model	Wavelength	
	20 cm	3 cm
1. Simple, Direct	257.4°K	295.0°K
2. Peake	253.2°K	296.4°K
3. de Loor and Meijboom	240.1°K	299.0°K

Background Soil Moisture Content = 15%
Vegetation Layer Thickness = 15 cm

As can be seen, the variations in brightness temperature response at λ = 3 cm due to different dielectric models are minimal (within 4°K). However, the differences at λ = 20 cm are quite substantial (up to 17°K). Therefore, an appropriate dielectric model for the vegetation layer at longer wavelengths is essential. The dependence of dielectric constant at 20 cm is also demonstrated in Figure 3-1 which shows the similar variation for various vegetation thicknesses. Assumptions of plant density water content and biomass are the same as in Table 3-1. The dependence on dielectric coefficients diminishes as vegetation thickness exceeds 150 cm.

3.3 Model of Volume Scattering for a Vegetation Medium

The effects of hydrometeors on microwave radiation are closely related to the particle size relative to the wavelength, an effect frequently described in terms of the non-dimensional size parameter, $q = 2\pi r/\lambda$, where r is the radius of the particle and λ is the wavelength. When q is very small ($<<1$), the effects are due primarily to absorption and can be treated as a function of liquid water content only. This condition applies for cloud droplets (typically of size less than 100 μm) at wavelengths longer than a few millimeters. For wavelengths in the submillimeter region, scattering effect of cloud particles has to be considered. For rain and surface snow, particle sizes are generally less than 1000 μm, therefore, volume scattering effect is important at wavelengths shorter than a centimeter. For a vegetation medium, it is expected that the volume scattering effect is important at wavelengths shorter than a few centimeters. The actual scattering effect of a vegetation medium is yet to be determined. The reasons are (1) it is difficult to understand the microstructure of a plant; the particles are non-spherical and cluttered, and (2) the distribution of plants within the vegetation medium is highly complex and random. There have been various modeling efforts of the scattering properties of various types of vegetation. For example, Chuang et al. (1980) employed the concept of correlation lengths in the horizontal and vertical directions resulting in a solution dominated by the forward scattering. Fung (1979) treated the vegetation layer as a volume of leaves and modeled it as an inhomogeneous medium with relative random permittivity function. Basharinov

et al. (1980) derived the vegetation model by combining surface scattering between the vegetation and the air and the volume scattering derived from a stochastic model comprising spatial variations in the dielectric constant.

In this study, effort was not placed in the area of defining the scattering properties of a vegetation layer. Instead, the resultant scattering effect on the observed microwave signature was investigated. Two aspects are considered: the response as a function of degree of scattering and its wavelength dependence.

A model was developed by Burke, et al. (1979) for treating multiple scattering processes for microwave-infrared atmospheric retrievals. In this study, it is further modified for a vegetation medium. The input parameters include:

1) equivalent dielectric coefficient for the vegetation medium and the wavelength of observation to derive the absorption coefficient (γa);

2) thickness of vegetation layer to obtain the total absorption thickness of the medium ($\gamma a * Z$);

3) physical temperature of the vegetation medium;

4) an equivalent single scattering albedo (ω); defined as the ratio of scattering (γs) to extinction ($\gamma a + \gamma s$). The value of ω can vary between 0 (no scattering) and 1 (full scattering); and

5) background soil conditions to derive the soil emmisivity.

The model is summarized in Appendix B.

Figure 3-2 is a plot of nadir brightness temperature response at λ = 20 cm as a function of vegetation depth. The complex dielectric coefficient of the vegetation layer is assumed to be (1.3, 0.022) as shown in Table 3-1 using the de Loor and Meijboom model. Three scattering albedos are considered: ω = 0, 0.2 and 0.5. ω = 0 case is equivalent to the dielectric slab (absorption only) model described in the previous section. The ω = 0.2 case produces a cooling effect of the

brightness temperature by a few degrees. The $\omega = 0.5$ case produces a cooling effect of $\sim$10°K for vegetation thicknesses less than 50 cm and 30°K for thicker vegetation. Comparing the data at 21 cm as presented in Section 2, scattering effect due to vegetation was minimal. Data observed from other experiments (e.g., Kirdyasher et al., 1979) also indicated that at L-band wavelengths the volume scattering effect can be neglected.

At shorter wavelengths, the volume scattering effect is found to be strongly related to the scattering albedo but relatively independent of the vegetation layer thickness. The effect of volume scattering is shown in Figure 3-3 for $\lambda = 3$ cm. The nadir brightness temperature is plotted as a function of the single scattering albedo (ω) of the vegetation medium. Compared with data at 2.8 cm as presented in Section 2, a scattering effect equivalent to $\omega = .3$ to .4 was evident due to the cooling of 20-30°K of the observed brightness temperature from the physical temperature.

Two conclusions are reached from the vegetation model and its application to data: (1) at L band wavelength, the background soil moisture information can still be retrieved; for the vegetation effect on observed signature, volume scattering is minimal, but the definition of the dielectric coefficient is important; and (2) at X and K band wavelengths, the background soil moisture information is generally obscured through a vegetation layer. Furthermore, vegetation layer also produces a strong multiple scattering effect within the medium, thus producing a cooling effect on the observed brightness temperature as compared to the actual physical temperature.

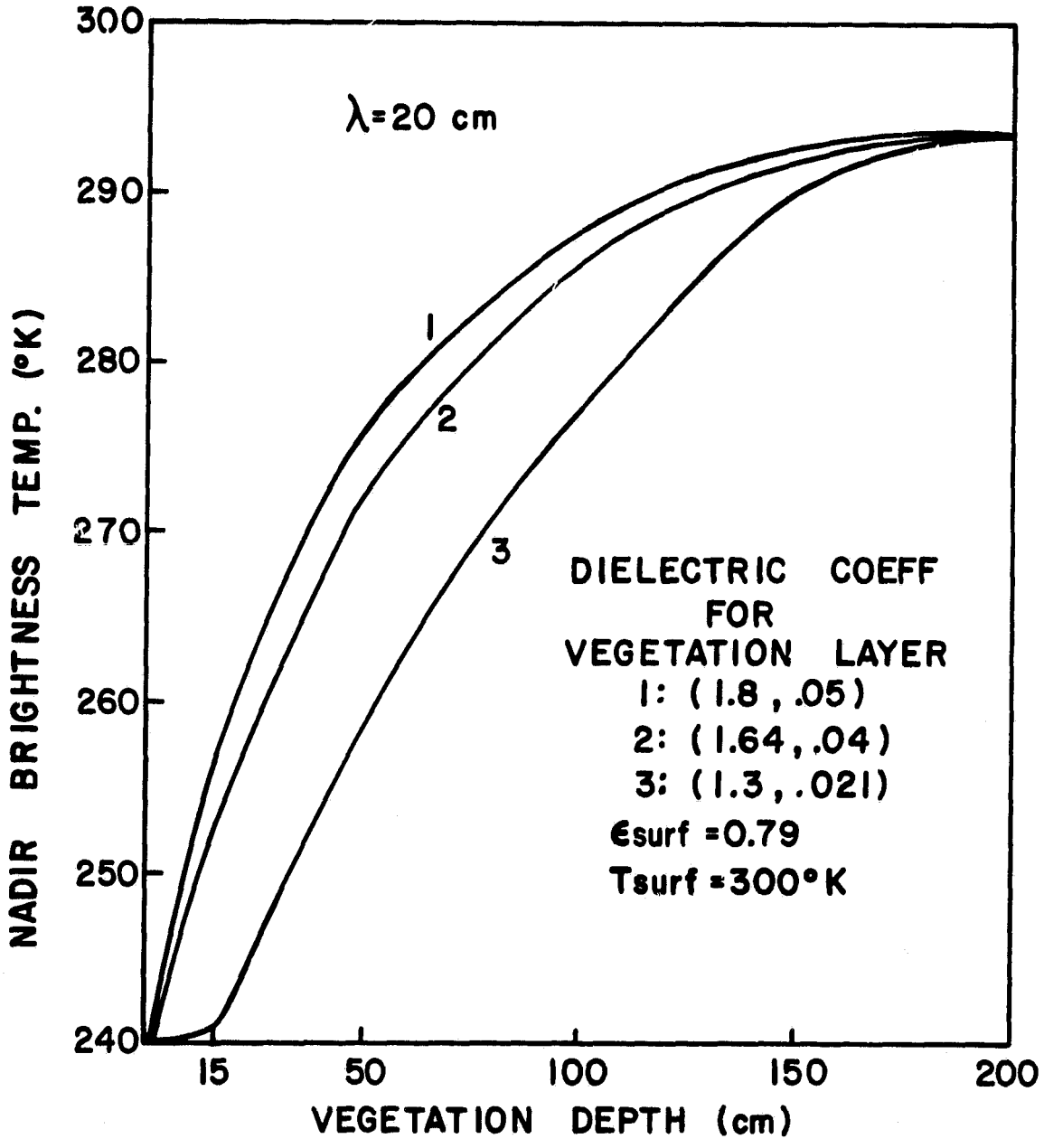

Figure 3-1 Response of a nadir brightness temperature at λ = 20 cm as a function of vegetation depth for three different dielectric models of the vegetation layer

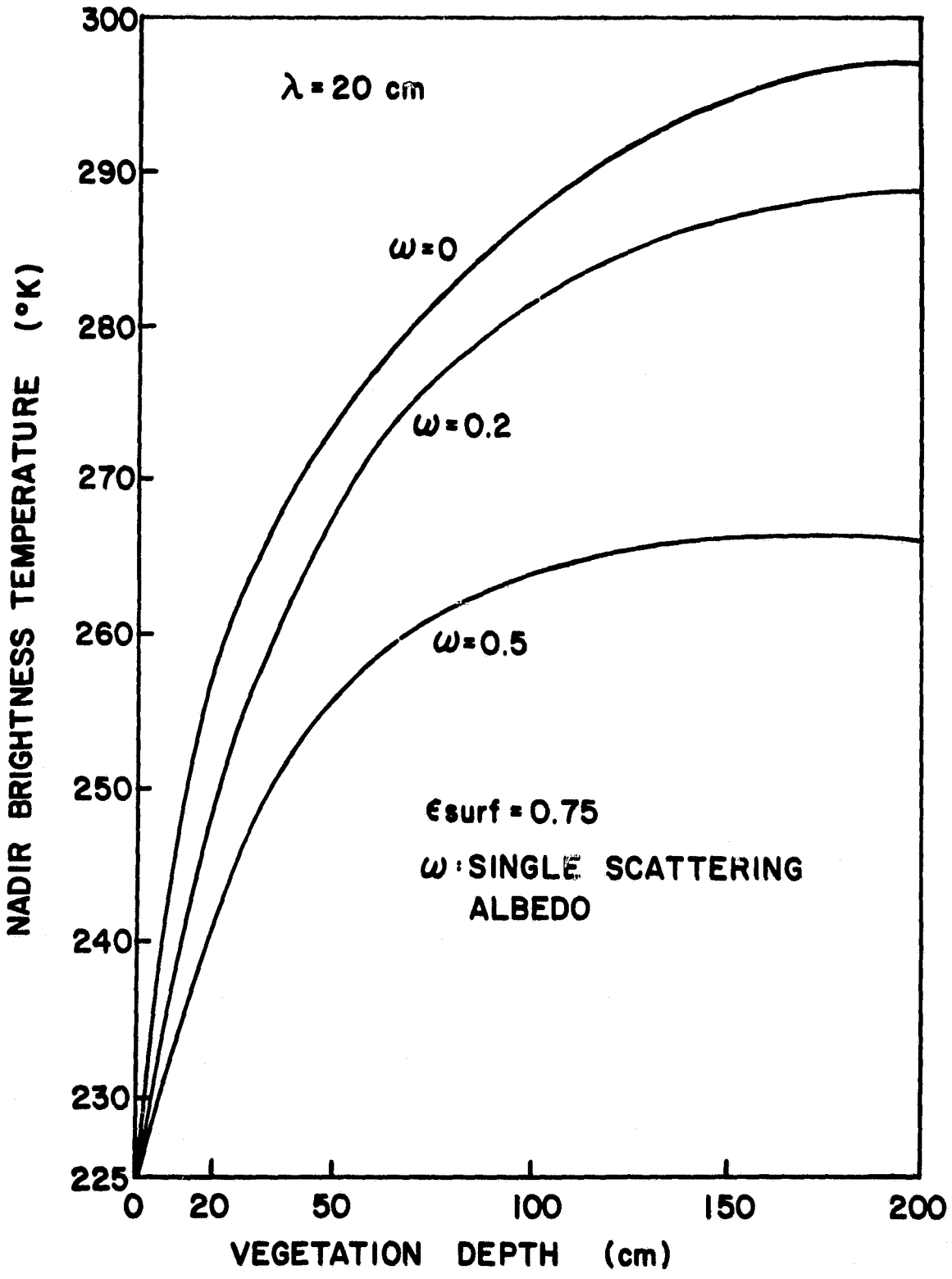

Figure 3-2 Response of a nadir brightness temperature at λ = 20 cm as a function of vegetation depth applied to three cases with different scattering effect

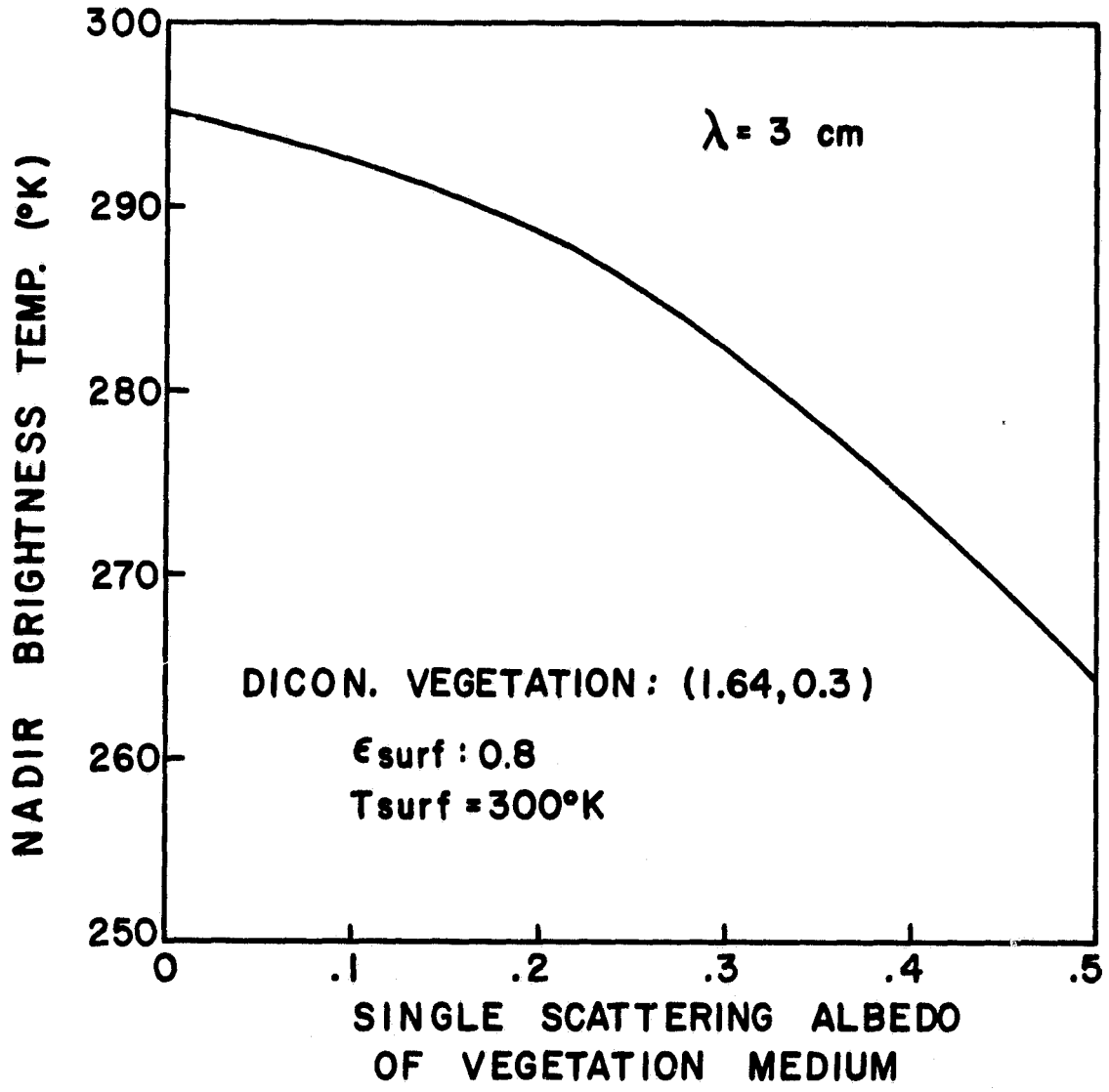

Figure 3-3 Response of a nadir brightness temperature at λ = 3 cm as a function of the single scattering albedo of the vegetation medium

4. ATMOSPHERIC EFFECTS IN THE MICROWAVE REGION

In order to define the optimum sensor wavelengths for space borne measurements of soil moisture, various meteorological conditions have to be investigated at different frequencies to test their sensitivities to soil moisture conditions. An atmospheric-surface interaction radiative transfer model (Gaut and Reifenstein, 1971; and Burke et al., 1979) can be applied to obtain the expected brightness temperature measured from space. The contributions of the signature include: (1) the emission of the attenuated background surface, (2) the upward emission from the atmosphere, and (3) the reflection of the downward atmospheric emission from the surface. The atmospheric parameters contributing to the microwave emission signature include water vapor and oxygen. In a cloudy or rainy atmosphere, additional parameters of liquid water and ice crystals have to be considered.

Three meteorological conditions are considered: (1) a standard tropical atmosphere with surface temperature of 300°K and relative humidity of 75%, (2) same atmosphere with a 2 km cumulus cloud from 1.5 to 3.5 km density of 0.4 gm/m^3, and (3) same atmosphere with a rain layer up to 4 km level and rain rate of 5 mm/hr. Wavelengths of 20, 5, 3, and 1.5 cm are tested with background surface moisture content varying from 5 to 35% (including a roughness factor of h = 0.4). Wavelengths shorter than 1.5 cm are not considered as they are not applicable for soil moisture monitoring due to their short skin depths. The results are outlined in Table 4.1. As can be seen, atmospheric effects at 20, 5, and 3 cm are minimal under all meteorological conditions considered. At 1.5 cm, rain conditions can affect the sensitivity to soil moisture conditions. However, under cloudy conditions, the soil moisture information can still be obtained. In conclusion, atmospheric effects generally do not create ambiguities of the soil moisture information at wavelengths optimal for soil moisture application.

TABLE 4.1

BRIGHTNESS TEMPERATURES OBSERVED FROM SPACE
THROUGH VARIOUS METEOROLOGICAL CONDITIONS AND SOIL MOISTURE CONTENTS

λ	Soil Moisture / Conditions	5%	15%	25%	35%
20 cm	clear	277.0	244.1	213.8	198.2
	cloud	277.0	244.1	213.8	198.2
	rain	276.6	243.7	213.4	197.8
5 cm	clear	284.0	244.6	226.6	218.8
	cloud	284.1	245.0	227.1	219.4
	rain	283.1	244.5	226.9	219.3
3 cm	clear	284.1	245.1	227.3	219.5
	cloud	284.3	246.2	228.8	221.3
	rain	281.0	246.3	230.5	223.6
1.5 cm	clear	285.9	254.6	240.3	234.0
	cloud	286.6	259.3	246.9	241.5
	rain	263.3	248.1	241.1	238.1

5. CONCLUSIONS

During the course of this study, three tasks related to soil moisture sensing at microwave wavelengths have been undertaken: (1) analysis of the 1975 flight data at L, X and Ku band wavelengths from Phoenix, Arizona, (2) modeling of vegetation canopy at microwave wavelengths and (3) investigation of atmospheric effects at these wavelengths. In essence, information obtained from longer wavelengths (e.g., L to C band) can be directly applied to retrieving soil information. For shorter wavelengths (e.g., X, K bands) the information of surface emissivity is also important for atmospheric retrievals.

Data from bare and vegetated fields included a broad range of soil moisture contents. Generally, the data agree well with theoretical estimates from a combined multilayer radiative transfer model with simple roughness correction. Secondly, the polarization parameters $P = \frac{1}{2}(T_{BV} + T_{BH})$ and $Q = (T_{BV} - T_{BH})$ are looked into. It is shown that P is closely related to the nadir brightness temperature and is more sensitive to soil moisture content than either T_{BV} or T_{BH}. Data of Q as a function of soil moisture content show a large scatter and therefore may not be useful for soil moisture retrieval. Further investigation should be carried out for studying its quantitative relationship to the surface roughness.. Thirdly, the possibility of detecting subsurface moisture information is also investigated by analyzing the predawn and afternoon data from combined 21 cm and 1.67 cm on two separate days throughout a drying cycle of the fields.

The modeling of vegetation is carried out by considering both the effect of dielectric coefficient and the volume scattering characteristics of the vegetation layer. It is concluded that at longer (e.g. L, S and C band) wavelengths the radiation from soil can still penetrate through vegetation layer providing sufficient surface moisture information. The key factor for determination of vegetation effect is the definition of dielectric coefficient. Volume scattering effect on these long wavelengths is minimal. At shorter wavelengths, it is concluded that radiation from soil cannot penetrate through a vegetation canopy. The key element controling the signature from a vegetation layer is its volume scattering characteristics.

The atmospheric effect at microwave wavelengths which are sensitive to soil moisture information is also investigated. Clear, cloudy and rainy conditions are considered at wavelengths of 20, 5, 3 and 1.5 cm. It is demonstrated that meteorological effects can generally be regarded as minimal except at shorter wavelengths under extreme weather conditions.

There are two scientific presentations and papers accomplished under the contract: (1) Feasibility of Detecting Subsurface Moisture Content Utilizing Multi-Frequency Microwave Radiometers (paper given at AGU, Washington, D.C., 1979), and (2) Requirements of Space-Borne Microwave Radiometers for Detecting Soil Moisture Contents (paper given at the Satellite Hydrology Symposium, Sioux Falls, S. Dakota, 1979).

ERT is currently under another contract, as a continuation of this study, to evaluate statistically the surface and subsurface soil moisture retrievability from past data. This should provide more findings on the possibility of detecting subsurface moisture information and also the expected accuracies.

Further research efforts should include the understanding of the causes of volume scattering effects of a vegetation medium by investigating the elements that contribute to them. This could then lead to the possibility of identifying various vegetations and their growth conditions at microwave wavelengths.

REFERENCES

Attema, E.P.W. and F.T. Ulaby, 1977: Vegetation Modeled as a Cloud Water, Radio Science, 13 (2), 357.

Burke, H.K. and W.J. Burke, 1979: Feasibility of Detecting Subsurface Moisture Content Utilizing Multi-frequency Microwave Radiometers, Trans. Amer. Geophys. U., 262.

Burke, H.K. and W.J. Burke, 1979: Prospects and Requirements for Spaceborne Microwave Radiometers for Detecting Soil Moisture Contents of Agriculture Fields. Proceedings, Satellite Hydrology of 1979 AWRA sponsored Pecora Symposium.

Burke, H.K., R.K. Crane, M.G. Fowler and R.D. Rosen, 1979: Microwave Infrared Retrievals, AFGL-TR-79-0019, Air Force Geophysics Lab., Hanscom Air Force Base, Massachusetts.

Burke, W.J., T. Schmugge and J.F. Paris, 1979: "Comparison of 2.8- and 21-cm Microwave Radiometer Observations Over Soils with Emission Model Calculations", J. Geophys. Res., 84, 287.

Basharinov, A.E., E.N. Zotova, M.I. Naumov and A.A. Chukhlantsev, 1980: Radiation Characteristics of Vegetation in the Microwave Band, Telecommunications and Radio Eng., (5), 69.

Choudhury, B.J., T.J. Schmugge, A. Chang and R.W. Newton, 1979: Effect of Surface Roughness on the Microwave Emission from Soils, Geophys. Res., 84 (9), 5699.

Chuang, S.L., J.A. Kong and L. Tsang, 1980: Radiative Transfer Theory for Passive Microwave Remote Sensing of a Two-Layer Random Medium with Cylindrical Structures, accepted by the J. Atm. Phys.

Fung, A.K., 1979: Scattering from a Vegetation Layer, IEEE Transactions on Geoscience Electronics, GE-17, 1.

Kirdyashev, K.P., A.A. Chukhlantsev and A.M. Shutko, 1979: Microwave Radiation of the Earth's Surface in the Presence of a Vegetation Cover, Radio Engineering and Electronic Physics, 2, 37.

deLoor, G.P. and F.W. Meijboom, 1966: The Dielectric Constant of Foods and Other Materials with High Water Contents at Microwave Frequencies, J. Fd. Technol., 1, 313.

Peak, W.H., 1959: Interaction of Electromagnetic Waves with some Natural Surfaces, IRE Transactions on Antennas and Propagation, AP-7, 5324.

Schmugge, T.J., B.J. Blanchard, W.J. Burke, J.F. Paris and J.R. Wang, 1976: Results of Soil Moisture Flights During April 1974, NASA TN D-8199.

Stogryn, A., 1970: The Brightness Temperature of a Vertically Structured Medium, Radio Sci., 5, 1397.

ACKNOWLEDGMENTS

This study was carried out for NASA/GSFC under contract NAS5-25529. Computer programming effort was provided by Ms. Jean Hsien Ho. The author wishes to thank Dr. Thomas J. Schmugge, the technical monitor, for providing the reduced data of the 1975 Phoenix experiment and for his many helpful suggestions. Furthermore, constructive discussions with Mr. Shun Lien Chuang, Professor Jin Au Kong, both of M.I.T., and Dr. William J. Burke of the Air Force Geophysics Laboratory are also greatly appreciated.

APPENDIX A

MODEL FOR MICROWAVE RESPONSE TO SOIL MOISTURE CONTENT

Thermal microwave radiation in soils results from the random, microscopic current loops within the soil volume (Stogryn, 1970). The intensity of radiation energy at a given point depends on the local dielectric coefficient and the physical temperature of the soil. Moisture produces a marked increase in both real and imaginary parts of the dielectric coefficient of soil, leading to a decrease in the soil's emissivity. This effect is mainly due to a lower transmission coefficient resulting from an increased dielectric mismatch between the regions of radiation generation (soil) and the point of observation (air). Experimental observations and theoretical calculations presented below indicate that emissivity of soils at microwave frequencies can range from >0.9 for dry soils to ≤0.6 for very moist soils.

In addition to the presence of moisture, surface roughness and vegetation cover also have significant effects, generally tending to increase the surface emissivity. Their effects will also be discussed in Section 3. In order to relate the microwave emissions measured by an aircraft or space vehicle antenna to the dielectric properties of the emitting soil, the following simplifying assumptions are made for the purpose of this paper:

(1) the radiation within the soil is incoherent,

(2) moisture and temperature are functions of depth only,

(3) dielectric and thermal properties of the soil are constant across layers of finite thickness, and

(4) the surface of the soil is smooth.

A cross section of a stratified soil is shown in Figure 1. Layers have thicknesses ΔZ_j. The jth layer is bounded on the top by the jth surface and by the j+1th surface on the bottom. Within this layer, the dispersion relation for electromagnetic wave propagation is $k_j^2 = (\omega/c)^2 \mu_j \xi_j$. In this equation, ω is the frequency in radians/sec, c is the velocity of light, μ is the magnetic permeability (assumed equal to one) and $\xi_j = \varepsilon_{Rj} + i\varepsilon_{Ij}$ is the complex dielectric coefficient. If we write

$k_j = \frac{\omega}{c}(\beta_j + ia_j)$, the the dispersion relation gives

$$\left(\beta_{xj}^2 + \beta_{yj}^2 + \beta_{zj}^2\right) - \left(a_{xj}^2 + a_{yj}^2 + a_{zj}^2\right) = \epsilon_{Rj}$$
$$2\beta_j \cdot a_j = \epsilon_{Ij} \tag{1}$$

and

It can be solved using Snell's Law to give

$$\beta_{zj} = \left[\frac{1}{2}\left(\epsilon_{Rj} - \mathrm{Sin}^2\theta_0\right)\left(1+\sqrt{1+\frac{\epsilon_{Ij}^2}{\left(\epsilon_{Rj} - \mathrm{Sin}^2\theta_0\right)^2}}\right)\right]^{\frac{1}{2}} \tag{2}$$
$$a_{zj} = \epsilon_I / 2\beta_{zj}$$

At the boundary between the j and j-1 layers, radiation is partially reflected and transmitted. The fractions of the incident electric field with horizontal and vertical polarizations reflected back into the jth layer are given by the Fresnel coefficients.

$$\rho_H = \frac{k_{zj} - k_{zj-1}}{k_{zj} + k_{zj-1}}$$
$$\rho_V = \frac{\xi_{j-1} k_{zj} - \xi_j k_{zj-1}}{\xi_{j-1} k_{zj} + \xi_j k_{zj-1}} \tag{3}$$

where $k_{zj} = \beta_{zj} + ia_{zj}$. Thus β_z, a_z, ρ_H and ρ_V all depend on the complex dielectric coefficient and the angle Θ_o that the ray emerges from the soil.

Within the first layer, the radiative transfer equation can be written as

$$\frac{d\, I_\omega}{dz} = -\gamma_1 I_\omega + \gamma_1 J_\omega \tag{4}$$

γ is the product of the density and monochromatic mass absorption coefficient. By writing the Poynting theorem in an appropriate form, it can be shown that $\gamma_i = 2\omega a_{zi}(\Theta_o)/c$.

I_ω is the intensity of radiation at frequency ω. J_ω is the Planck emission function. In the microwave frequency range, Planck's emission law reduces to the Rayleigh-Jeans equation, where J_ω is proportional to the temperature of the medium T. Adopting a similar scaling rule for I_ω, an effective temperature T_p can be defined which is directly proportional to I_ω. The subscript ω is suppressed and T_p refers to the intensity in a narrow range near ω in the p polarization state. Since J_ω is isotropic and independent of polarization, no designation is necessary. The radiative transfer equation in the first layer may be written:

$$\frac{dT_p}{d(\gamma_i z)} = -T_p + T_i \tag{5}$$

This equation can be integrated from a point just below the surface to a point just above the interface between the first and second layers. Because the dielectric properties are assumed to be constant across the layer

$$T_p(1^-) = T_1 \left(1-e^{-\gamma_1 \Delta z_1}\right) + T_p(2^+)e^{-\gamma_1 \Delta z_1} \tag{6}$$

The argument $N^{\pm}$ implies that the measurement is made above (+) or below (-) the Nth interface. The first term on the right hand side of equation 6 accounts for radiation emitted within the first layer and comes directly to the surface. The second term describes upwelling radiation at the bottom of the first layer. This in turm has two components: first, radiation emitted in the first layer and reflected at the interface between the first and second layers; and second, radiation transmitted from lower layers.

Repeating the procedure of integrating the radiative transfer equation for N layers, the brightness signature right above the surface can be shown as

$$T_p(1^+,\theta_0) = \sum_{i=1}^{N} T_i \left(1-e^{-\gamma_i(\theta_0)\,\Delta z_i}\right) \left(1+R_{p,i+1}(\theta_0)\, e^{-\gamma_i(\theta_0)\,\Delta z_i}\right) \prod_{j=1}^{i} (1-R_{pj}(\theta_0))\, e^{-\left(\sum_{j=2}^{i} \gamma_{j-1}(\theta_0)\,\Delta z_{j-1}\right)} \tag{7}$$

An atmospheric-surface interaction radiative transfer model (Gaut and Reifenstein, 1971; and Burke et al, 1979) is then applied to obtain the expected brightness temperature measured from space. The contributions of the signature include: (1) the emission of the attenuated background surface, (2) the upward emission from the atmosphere, and (3) the reflection of the downward atmospheric emission from the surface. The atmospheric parameters contributing to the microwave emission signature include water vapor and oxygen. In a cloudy or rainy atmosphere, additional parameters of liquid water and ice crystals have to be considered.

APPENDIX B

A SOLUTION TO THE RADIATIVE TRANSFER EQUATION WITH MULTIPLE SCATTERING EFFECT

The inclusion of vegetation in the radiative transfer equation complicates the problem due to the addition of volume scattering effect. Instead of the nonlinear quadrature formula represented by equation (A-4), the radiative transfer equation becomes an integral equation incorporating the effects of multiple scattering. Numerical solutions to the multiple scattering equations have been available for some time but the procedures have been time consuming and costly to operate. With the variational-iterative method developed at ERT, computer times are short enough and costs low enough to permit the inclusion of multiple scattering effects in the radiance computation. To apply it to the microwave response to vegetation, the Planck function is replaced by the physical temperature and the intensity by the brightness temperature.

Variational-Iterative Method

The radiative transfer equation for a plane-parallel scattering atmosphere is given by (Chandrasekhar, 1960):

$$\mu \frac{dI_\nu(\tau,\mu,\phi)}{d\tau} = I_\nu(\tau,\mu,\phi) - J_\nu(\tau,\mu,\phi)$$

where $$J_\nu(\tau,\mu,\phi) = \frac{1}{4\pi}\int_{-1}^{+1}\int_{o}^{2\pi} p(\mu,\phi;\mu^1,\phi^1) I_p(\tau,\mu^1,\phi^1) d\mu^1 d\phi^1$$

$$+ J_o(\tau,\mu,\phi)$$

μ is the cosine of the zenith angle

ϕ is the azimuth angle

J is the source function

J_o is the primary exitation source function

p is the phase function

and the remaining symbols were defined above. For a scattering plane-parallel atmosphere with the primary source emission from atmospheric gasses or for a plane-parallel atmosphere with an external source (the sun say) and isotropic scattering, the problem has axial symmetry about the zenith direction and the dependence on azimuth can be removed:

$$\mu \frac{dI(\tau,\mu)}{d\tau} = I(\tau,\mu) - J(\tau,\mu) \tag{1}$$

$$J(\tau,\mu) = J_o(\tau,\mu) + \frac{1}{2} \int_{-1}^{1} p(\mu,\mu^1) I(\tau,\mu^1) d\mu^1 \tag{2}$$

where the explicit dependence on ν has been suppressed.

The phase function is normalized to represent the total energy scattered by a single scatter relative to the sum of the energy absorbed and scattered by the particle:

$$\frac{1}{4\pi} \int_{-1}^{1} \int_{o}^{2\pi} p(\mu,\phi;\mu^1,\phi^1) d\mu^1 d\phi^1 = \omega_o \leq 1 \tag{3}$$

where ω_o is the single scattering albedo. For an isotropic scatterer, p = constant = ω_o. The primary exitation source function for atmospheric thermal emission is

$$J_o(\tau) = (1 - \omega_o(\tau)) B[T(\tau)] \tag{4}$$

where $B[T(\tau)]$ is B_ν, the Planck function. In this representation of the radiative transfer equation, the distance from the top or bottom of the atmosphere is measured in units of optical depth, τ, rather than distance or pressure. The point properties of the medium such as the single scattering albedo are then functions of τ.

$$\tau(\zeta) = \int_{\zeta}^{\infty} \gamma_e(\zeta)d\zeta \tag{5}$$

$$\omega_o(\zeta) = \frac{\gamma_e(\zeta) - \gamma_a(\zeta)}{\gamma_e(\zeta)} \tag{6}$$

where γ_e is the volume extinction coefficient (cross section per unit volume)

γ_a is the absorption coefficient as defined above and ζ = height.

From equations (3), (4) and (5), the source function can be written as

$$J(\tau) = 1 - \omega_o(\tau))B(T(\tau)) + \frac{\omega_o(\tau)}{2}\int_o^{\tau^*} J(\tau)E_1(|\tau-\tau^*|)d\tau$$
$$+ \frac{\omega_o(\tau)}{2}\int_o^1 I(\tau^*,\mu^1)e^{-(\tau^*-\tau)/\mu^1}d\mu^1 \tag{7}$$

where E_1 is the exponential integral of the first order and

τ^* is the total optical depth such that $I(\tau^*,\mu)$ is the outgoing (upwelling) intensity at the lower boundary (surface).

The exponential integral E_n of the nth order is defined as

$$E_n(x) = \int_o^1 e^{-x/\mu}\mu^{n-2}d\mu;\ n = 1,\ 2\cdots$$

$I(\tau^*,\mu)$ has two contributions: (1) surface emission and (2) surface reflection. For a surface reflectivity, R, and temperature, T_s,

$$I_1(\tau^*,\mu) = (1 - R)B(T_s) \tag{8}$$

$$I_2(\tau^*,\mu) = 2\cdot R\cdot \int_o^1 I(\tau^*,-\mu^1)\mu^1 d\mu^1 \tag{9}$$

where $I(\tau^*,-\mu^1)$ is the downward intensity at the surface in the direction corresponding to μ^1.

Equation (13) is based on the assumption of a Lambertian surface; there will be an "isotropic" reflection independent of the incident angle on the surface. Equation (13) can further be written as

$$I_{(2)}(\tau^*,\mu) = 2 \cdot R \cdot \int_0^{\tau^*} J(t)\, E_2(\tau^* - t)dt \tag{10}$$

where E_2 is the second order exponential integral. Combining (7), (8) and (9) we obtain the expression for the source function:

$$\begin{aligned} J(\tau) &= (1 - \omega_o(\tau))B(T(\tau)) + \frac{\omega_o(\tau)}{2} \int_0^{\tau^*} J(t)E_1(|t-\tau|)dt \\ &+ \frac{\omega_o(\tau)}{2} \cdot E_2(\tau^*-\tau)[(1-R)B(T_{gr}) + 2 \cdot R \cdot \int_0^{\tau^*} J(t)E_2(\tau^*-t)dt] \end{aligned} \tag{11}$$

The outgoing intensity at the top of the atmosphere then can be expressed as

$$\begin{aligned} I(0,\mu) &= \int_0^{\tau^*} J(t)e^{-t/\mu}dt/\mu + (1-R)B(T_{gr})e^{-\tau^*/\mu} \\ &+ 2 \cdot R \cdot [\int_0^{\tau^*} J(t)E_2(\tau^*-t)dt]e^{-\tau^*/\mu} \end{aligned} \tag{12}$$

The three terms on the right hand side of equation (12) are

(1) the upward emission from the vegetation and atmosphere,

(2) the emission of the attenuated background surface, and

(3) the reflection of the downward atmospheric/vegetation emission from the surface.

The variational-iterative (VI) approach (Sze, 1976) is used to solve this system of equations. The variational method depends on finding the "extremum" of a certain functional; an a priori form is used for the unknown function and the coefficients are found from a set of minimizing conditions. In essence, this method provides a direct way for constructing an approximate solution for the source function. The atmosphere is divided into subintervals and the source function is approximated as a combination of step functions in different intervals. The advantages of this technique are that: (1) it is fast and requires

little computational time to achieve satisfactory accuracy, and (2) it allows vertical inhomogeneity and the inclusion of surface reflection.

The VI technique provides a direct method for constructing an approximate solution to the integral equation (11) for the source function. An approximate source function can be expressed as

$$J_a(\tau) = U_a(\tau)\sqrt{\omega_o(\tau)} \tag{13}$$

where

$$U_a(\tau) = \sum_{i=1}^{N} C_i V_i(\tau)$$

and the $V_i(\tau)$ are known trial functions. The choice of trial functions plays an important role in the ultimate success of the variational method (Kourganoff, 1963). In the variational solution employed by Sze, simple step functions were chosen as the trial functions. This choice (1) makes it simple to perform the integrals required in (11) and (2) the intervals can be chosen to resemble multiple cloud layers, the weights $C_i\sqrt{\omega_i}$ for each layer represent the average source function in that layer where ω_i is the single scattering albedo for the layer.

The total optical depth τ^* is divided into N-1 intervals with ω_i constant over each interval. The trial function then is

$$V_j(\tau) = \begin{cases} 1 & \tau_j < \tau \leq \tau_{j+1} \\ 0 & \text{otherwise} \end{cases} \tag{14}$$

The C_i then are solutions of the algebraic equation

$$\sum_{j=1}^{N} M_{ij} C_j = f_i \tag{15}$$

where

$$M_{ij} = \delta_{ij}\Delta\tau_j - \sqrt{\frac{\omega_i\omega_j}{2}} \int_{\tau_i}^{\tau_{i+1}} D_j(\tau)d\tau \tag{16}$$

$$\delta_{ij} = \begin{cases} 0, & i \neq j \\ 1, & i = j \end{cases}$$

$$D_j(\tau) = \int_{\tau}^{\tau_{j+1}} E_1(|\tau - t|)dt$$

and $$f_i = \left(\frac{1-\omega_i}{\sqrt{\omega_i}}\right) B(T(\tau_i)) + \frac{\sqrt{\omega_i}}{2} E_2(\tau^* - \tau_i)\ (1-R)B(T_s) \qquad (17)$$

The variational solution is an approximation to the actual solution which is correct at least at one level within each layer (Sze, 1976). A smoothed approximation for the source function then can be constructed:

$$J_1(\tau) = (1-\omega_o(\tau))B(T(\tau)) + \frac{\omega_o(\tau)}{2} E_2(\tau^* - \tau)(1-R)B(T_s)$$

$$+ \frac{\omega_o(\tau)}{2} \sum_{j=1}^{N-1} C_j \sqrt{\omega_j(\tau)}\ D_j(\tau) \qquad (18)$$

$$+ \omega_o(\tau)\ E_2\ (\tau^* - \tau)\ R \sum_{j=1}^{N-1} C_j \sqrt{\omega_j(\tau)} \int_{\tau_j}^{\tau_{j+1}} E_2(\tau^* - t)dt$$

Since the smoothed approximation is a summation over layers with oscillating residual errors, it provides a reasonable first estimate of the true source function (Burke and Sze, 1977). Improved accuracy may be obtained by further iterations of the integral equation for the source function as:

$$J_{n+1}(\tau) = (1-\omega_o(\tau))B(T(\tau)) + \frac{\omega_o(\tau)}{2} E_2(\tau^* - \tau)(1-R)B(T_s)$$

$$+ \frac{\omega_o(\tau)}{2} \int_0^{\tau^*} E_1(|\tau - t|)J_n(t)dt \qquad (19)$$

$$+ \omega_o(\tau)\ E_2(\tau^* - \tau)\ R \int_0^{\tau^*} E_2(\tau^* - t)J_n(t)dt$$

The residue of the nth iteration is defined as

$$\Delta_n = \left|\frac{J_n - J_{n-1}}{J_n}\right| \qquad (20)$$

By specifying the maximum residue allowed, the iteration process then brings the source function to desired accuracy. The number of iterations for the system also depends on the choice of the number of step functions